3

# Hydraulic Conductivity and Water Retention Curve of Highly Compressible Materials- From a Mechanistic Approach through Phenomenological Models

Serge-Étienne Parent[1], Amir M. Abdolahzadeh[2], Mathieu Nuth[3] and Alexandre R. Cabral[4]
[1]*Department of Soils and Agrifood Engineering, Université Laval, (Formerly, Ph.D. student, Université de Sherbrooke),*
[2,3,4]*Department of Civil Engineering, Université de Sherbrooke, Canada*

## 1. Introduction

Highly compressible material (HCM), such as clay and materials containing high organic content, are increasingly used for applications in geoenvironmental engineering and agriculture (Nemati, et al., 2002; Paquet & Caron, 1993). In particular, deinking by-products (DBP) - a clay and fibers spongy material produced in the early stage of the paper recycling process - has been suggested by numerous authors as a cover material over landfills (Kraus, et al., 1997; Moo-Young & Zimmie, 1996; Cabral, et al., 1999; Burnotte, et al., 2000; Kamon, et al., 2002; Parent, 2006; Robart, 1998; Bédard, 2005) and mine waste top covers (Cabral, et al., 1999) as well as structural enhancement material in agricultural soils (Nemati, et al., 2000). The challenge with using DBP as part of a landfill cover was reviewed by Cabral et al. (2007) and Abdolahzadeh et al. (2010; 2008).

The unsaturated hydraulic properties of DBP are fundamental for the design of top covers. Those properties are namely water retention curve (WRC), also commonly called soil-water characteristic curve (SWCC[1]) and hydraulic conductivity function (*k*-function). In the early stage of our projects concerning DBP, we needed to determine their hydraulic properties. DBP revealed to be highly compressible under the effect of suction, and classical models to represent the WRC of porous materials (Brooks & Corey, 1964; van Genuchten, 1980; Fredlund & Xing, 1994) usually do not take into account volume change during drying. Indeed, when a porous material dries, the capillarity phenomenon induces a tensile stress into the pores. As a result, the pores may shrink upon drying. Variations in pore structure

[1] The expression "water retention curve" is preferred over the widely used "soil-water characteristic curve", because many porous materials, like DBP, are not soils. Moreover, to state that the water retention curve is characteristic may only be appropriate if it is use to distinct a porous material from others.

resulting from variations of suction would influence water retention characteristics, i.e. air-entry value (AEV), desaturation slope and residual trend.

Moreover, because of experimental difficulties involved in direct determination of the hydraulic conductivity function (*k*-function), the conventional practice is to indirectly estimate the *k*-function based on WRC models (Fredlund, et al., 2002; Huang, et al., 1998; Leong & Rahardjo, 1997; Fredlund, et al., 1994; Mualem, 1976). Huang et al. (1998) proposed a minor adaptation of the Fredlund et al. (1994) *k*-function model, derived from the Childs & Collis-George (1950) model. Reliability and validity of *k*-functions depends not only on the *k*-function model selected, but also on accuracy of the WRC model used to derive the *k*-function. As a result, there is a need for more suitable methods to determine the WRC and *k*-functions of HCMs.

This research project provides a mechanistic approach based on a compression energy concept accounting for pore shrinkage under the effect of suction. A clear distinction between non-compressible materials, compressible materials and highly compressible materials is also made. Highly compressible materials (HCMs) are defined as porous materials undergoing considerable strain as an effect of external stresses or internal pressure. For HCMs, tensile stresses will induce shrinkage even for suction levels greater than the AEV. An experimental technique was developed to determine the WRC of HCMs. The testing procedure was based on the axis-translation technique and allowed for simultaneous and continuous determination of the volumetric water content and void ratio of soil samples during desaturation (Cabral, et al., 2004). The results obtained from the developed testing procedure indicate that our material behave like a HCM.

In this chapter, a WRC model is proposed for suction-driven shrinkage of HCMs. The proposed model, based on a model originally proposed by Fredlund et al. (1994), was validated using experimental data published by Huang (1994). The results of representative tests to determine the WRC of DBP are discussed, as well as their associated computed k-functions.

This study also provides a procedure to determine the *k*-function of HCM, based on hydraulic conductivity tests performed on saturated samples and on suction test data performed in order to obtain the AEV. Suction tests must be performed so that volume changes can be monitored using methodologies such as proposed by Cabral et al. (2004). The procedure was validated by comparing results of actual unsaturated hydraulic conductivity tests (experimental data for a compressible soil published by Huang (1994) with predictions made by applying the procedure.

## 2. Definitions and concepts

Volume change is a change of porosity in response to a change in stress state (Fredlund & Morgenstern, 1976). A porous material can be compressed by either mechanical or suction-induced tensile stresses. A mechanical stress is defined as an external stress (i.e. a pressure exerted at the boundaries of a sample) or as a gravity-induced stress. A mechanical stress can thus be generated by a weight or an impact, and accentuated by vibration. Suction-induced tensile stresses rise from water menisci that attract particles to each other. Water suction ($\psi$) is a reactive pressure that equilibrates with pressure caused by gravitational forces, osmosis or pneumatic pressures. Osmotic suction will be dominant only at high suction ranges and are not considered in this report.

Pore shrinkage may happen during desaturation, resulting in modifications of hydraulic properties. In this section, a mechanistic theory for the compression of porous material is introduced, leading to a phenomenological model describing the water retention curve (WRC) of highly compressible materials (HCM) and a procedure to predict the hydraulic conductivity function (*k*-function) of HCM using saturated samples.

### 2.1 Porous material compression

Many authors showed that, as long as the pores are saturated, the compression processes induced by mechanical and suction stresses can be considered identical (Khalili & Khabbaz, 1998). However, unsaturated porous materials must behave differently (Toll, 1988).

#### 2.1.1 Saturated porous media

The principle of effective stress is probably the most fundamental in soil mechanics. In its general form, it is defined as the difference between total stress and pore water pressure (Holtz & Kovacs, 1981; Terzaghi, 1936), as follows:

$$\sigma' = \sigma - u \tag{1}$$

where σ′ is effective stress (kPa), $\sigma$ is net or total stress (kPa), $u$ is pore water pressure ($u = -\psi$) and $\psi$ is matric suction (kPa). We assume that stress is isotropic, and that $\sigma'$ designates the mean value of effective stress in this chapter, unless otherwise indicated. Note that $u_a$, the air pressure, is supposed to be the same for $\sigma$ and $u$.

As shown in the following sections, porosity (or void ratio) decreases with increasing total stress or decreasing pore pressure (increasing suction), but both stresses are acting differently on the pore structure.

#### 2.1.2 Unsaturated porous materials

For porous materials in the unsaturated state, variation in suction does not result in the same change in effective stress as the equivalent variation in applied mechanical stresses. In the case of a pressure state, a water pressure stress is applied on every particles of a porous material. However, when a porous material is under suction, the pores may not be fully saturated and tensile forces, that attract pore walls together, may not be applied over all the pores. Bishop (1959) proposed a factor $\chi$ that factors tensile stress under unsaturated conditions. This factor was later transformed to a function by Khalili & Khabbaz (1998), as follows:

$$\sigma' = \sigma - \chi(\psi)u = \sigma + \chi(\psi)\psi \tag{2}$$

where χ(ψ) is an effective stress function attaining the value of 1 for saturated porous materials and 0 when the porous material is completely dry (no units).

The Bishop's effective stress is often considered as a natural extension of the saturated effective stress to unsaturated soils (explained further in section 2.1.2.1). Equation 2 reveals that the external stress and the suction can both have an influence on the effective stress. The relevancy of the unsaturated effective stress has been questioned in the literature, especially regarding the phenomenon of wetting collapse. Recent works clarified the definition and implications (Jardine, et al., 2004; Nuth & Laloui, 2008) of Bishop's stress. They justified that

the latter is an adequate representation of the state of stress within the unsaturated soils, and a convenient constitutive stress variable.

The constitutive behavior of soils is complex due to the intrinsic non-linearities as well as irreversible phenomena (i.e. plasticity). For the sake of simplicity, only monotonic loading paths (drying tests) will be considered in the rest of the paper. This simplification allows us to use phenomenological models based on non linear elasticity. The modeling of cyclic test paths using the theory of elasto-plasticity is out of the scope of the paper. D'Onza et al. (2010) present a review of the recent, advanced models for unsaturated soils coping with elasto-plastic features.

Fredlund & Morgenstern (1976) proposed that Bishop (1959)'s equation describes a constitutive behavior of unsaturated soils. The planes plotted in Fig. 1 presents such behavior for a single material. Porosity (light gray plane in Fig. 1) decreases with both increasing suction and net stress, but the $\chi(\psi)$ function reduce the contribution of suction to shrinkage while the material desaturates. Compared to the WRC at low porosity, a WRC at high porosity is characterized by a lower air-entry value (AEV) and a steeper desaturation slope. Salager et al. (2010) considered the constitutive desaturation plane as a hydromechanical phenomenon and adopted the term "soil-water retention surface", contrasting with the usual expression "soil-water retention curve", the equivalent of the term "water retention curve" used in this report. Consequently, the WRC would be the projection of the "water retention plane" on the suction axis (dark plane in Fig. 1).

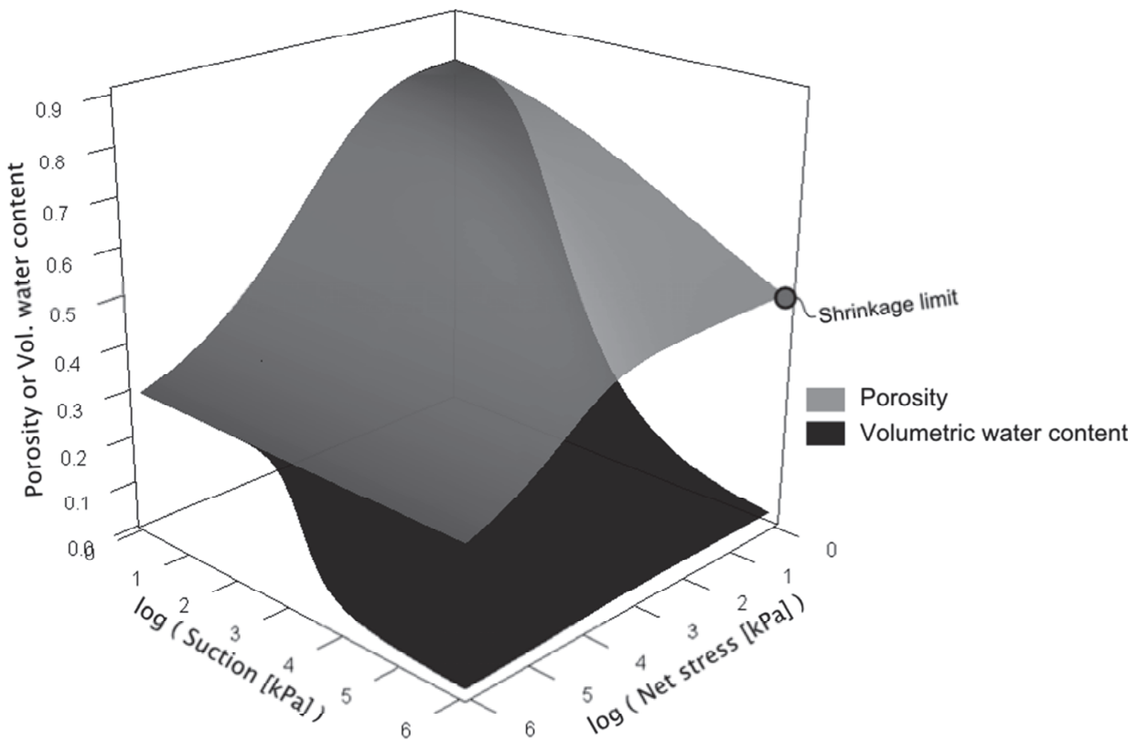


Fig. 1. Fredlund and Morgenstern constitutive model

**2.1.2.1 The capillary-induced compression energy**

Parent (2006) related the capillary induced volume change behavior with the concept of compression energy. Indeed, stress is by definition a volumetric concentration of energy:

$$Stress = \frac{Force}{Surface} = \frac{Force \times Distance}{Surface \times Distance} = \frac{Energy}{Volume} \tag{3}$$

or

$$kPa = \frac{kN}{m^2} = \frac{kN \cdot m}{m^2 \cdot m} = \frac{kJ}{m^3} \tag{4}$$

In order to collapse, a porous material needs an energy source that is able to contract the pores. This energy can be of two major sources:

- **Mechanical energy**: The sample is compressed under the effect of gravity. The effect can be accentuated thanks to a vibration energy, weight or impact. For example: the mass of an overlying soil, a vibrating compactor, a falling proctor hammer.
- **Capillary energy**: Drying a sample induces tensile internal stresses caused by water menisci, which forces particles to reorient and attract to each other, hence leading to shrinkage (Baumgartl & Kock, 2004). For example: (1) soil surfaces exposed to the sun may dry, shrink and crack, creating shriveled pattern, and (2) a strain may be observed on the slope of a drained, recently dug ditch.

Whereas the mechanically induced compression energy is distributed into the solid matrix of the porous material, the energy induced by capillary forces is distributed into the water phase contained in the pores of a porous material, as follows:

$$[E]_{mec} = \sigma \times \frac{V_s}{V_s} = \sigma \tag{5}$$

$$[E]_{cap} = \psi \times \frac{V_w(\psi)}{V_p(\psi)} = \psi \times S(\psi) \tag{6}$$

where $[E]_{mec}$ is the concentration of mechanically induced compression energy, $\sigma$ is the total (mechanical) stress, $V_s$ is the solid volume of a porous material sample, $[E]_{cap}$ is the concentration of capillary induced compression energy, $\psi$ is the suction, $V_w$ is the volume of water into a porous material sample, $V_p$ is the volume of the pores and $S(\psi)$ is the degree of saturation as a function of suction, or the water retention curve (WRC).

If the porous material is fully saturated, then Equation 6 yields that $[E]_{cap} = \psi$. This shows that the concentrations of mechanically and capillary induced energy are equivalent: for $\psi = \sigma$, $[E]_{cap} = [E]_{mec}$ as long as the porous material is saturated. The AEV is defined by the suction value where significant loss of water is observed on the $S$ versus $\psi$ curve, i.e. in the region of the inflection point determined using the procedure proposed by Fredlund & Xing (1994)[2]. Accordingly, when the largest pores of a material are drained, close to the AEV, $S(\psi)<1$. Thus, $[E]_{cap} < [E]_{mec}$. As Toll (1995) stated, for suction values higher than the AEV, the largest pores have been already compressed (shrinkage happens in the pores containing water). We may add that the finer pores need more energy to be compressed and are less susceptible to volume loss. For this reason, the shrinkage limit, which is defined as the stabilized, minimal volume of soil (see Fig. 1 and Fig. 2), is often assumed being reached at

[2] The tangent method (Fredlund & Xing, 1994) defines the AEV as the suction value in the inflection zone of the WRC on the degree of saturation scale where the projection of the desaturation slope crosses the degree of saturation value of 100%, generally determined on a log scale along the suction axis.

the AEV. Nevertheless, we infer in this chapter that for materials that are highly compressible, $[E]_{cap}$ may be sufficient to keep on inducing compression for suction values greater than the AEV. Hence, the shrinkage limit may be observed for suction values higher than the AEV.

From the compression energy concept, it can be inferred that $\chi(\psi)$ may be somehow related to $S(\psi)$. Indeed, the pore water pressure component of the effective stress ($\chi(\psi)\cdot\psi$) should null when the porous media is saturated ($\psi=0$ and $\chi=1$), and also be null when it is dry ($\psi = 10^6$ kPa - the theoretical suction value that corresponds to a null water content (Fredlund & Xing, 1994) - and $\chi=0$).Hence, the pore water pressure component of the effective stress in unsaturated state - i.e. $\chi(\psi)\cdot\psi$ - reaches a maximal value at a certain suction value between complete and null saturation. This behavior can be easily observed when wet and dry beach sands flows through our fingers, but when the sand is partially saturated, particles stick together, making possible the construction of a sand castle. However not supported by a mechanistic model, Bishop (1959)'s approach was used by Khalili & Khabbaz (1998), who proposed an exponential empirical relationship between $\chi$ and ratio $\psi/\psi_{aev}$ (where $\psi_{aev}$ is the AEV), allowing the determination of $\chi(\psi)$ for most soils with an equation similar to the one proposed by Brooks & Corey (1964) for WRC curve fitting:

$$\chi(\psi) = \begin{cases} \left(\frac{\psi}{\psi_{aev}}\right)^{\iota} & if \quad \psi \geq \psi_{aev} \\ 1 & if \quad \psi \leq \psi_{aev} \end{cases} \tag{7}$$

where $\psi_{aev}$ is the suction at the air-entry value (AEV) and $\iota$ is an empirical parameter estimated to be equal to -0.55 by Khalili & Khabbaz (1998).

It is possible to force parameter $\chi$ to reach a null value at $10^6$ *kPa* using the function $C(\psi)$ in Equation 10, presented after.

$$\chi = \begin{cases} \left(1 - \frac{ln\left(1+\frac{\psi}{C_r}\right)}{ln\left(1+\frac{\psi}{10^6}\right)}\right) \times \left(\frac{\psi}{\psi_{aev}}\right)^{\iota} & if \quad \psi \geq \psi_{aev} \\ 1 & if \quad \psi \leq \psi_{aev} \end{cases} \tag{8}$$

The optimum of compression capability by means of suction using $\chi$ is coherent with Fredlund (1967)'s conceptual behavior, that was treated later on by Toll (1995). The latter suggested that void ratio of a normally consolidated soil decreases as suction increases and levels off slightly after the AEV, *i.e.* where "[...] *the suction reaches the desaturation level of the largest pore (either due to air entry of cavitation) and air starts to enter the soil. The finer pores remain saturated and will continue to decrease in volume as the suction increases. However, the desaturated pores will be much less affected by further changes in suction and will not change significantly in volume. The overall change will therefore be less than in a mechanically compressed saturated soil, and the void ratio - suction line will become less steep than the virgin compression line*[3] ".

A schematic representation of Fredlund (1967)'s conceptual behavior is shown in. Fig. 2. As pores lose water under the effect of suction, porosity follows the virgin compression line and the water retention curve (WRC). Porosity stabilizes at suction values slightly higher than the AEV. The asymptote toward which the curve converges is the shrinkage limit.

[3] Toll (1995), page 807.

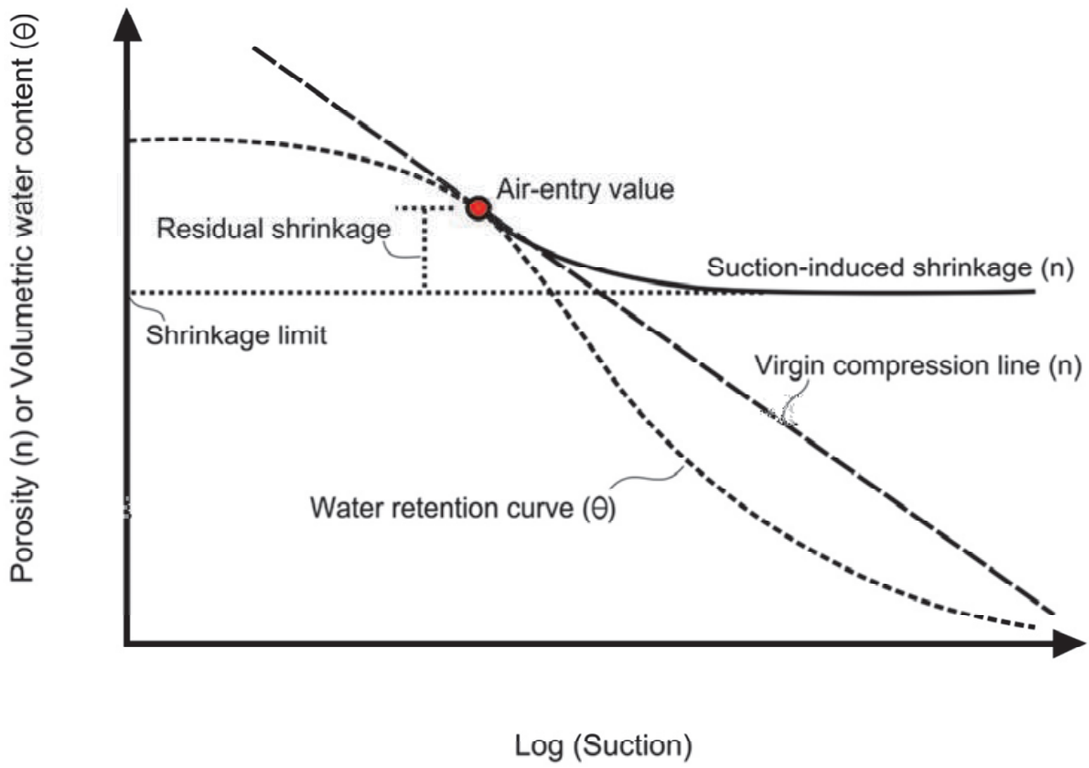


Fig. 2. Conceptual scheme representing shrinkage

Most data from the literature come from soils and show a shrinking behavior similar to the one schematically presented in Fig. 2, where the shrinkage limit is reached in the area of the AEV. However, it is shown by the compression energy concept (Equation 6) that capillary stresses are still active for suction values beyond the AEV. Fig. 3 shows a hypothetical desaturation curve and porosity function of a highly compressible material. The desaturation curve is expressed both in terms of volumetric water content and degree of saturation, the later being printed for sake of comparison with the $\chi(\psi)$ function (Equation 8). The concentration of capillary energy - $S(\psi)\cdot\psi$ - is plotted asides the suction component of the effective stress - i.e. $\chi(\psi)\cdot\psi$.

It can be observed that $S(\psi)$ is similar to the more generic $\chi(\psi)$ function (using $\iota$=-0.55), leading to similar $[E]_{cap}$ and $\chi(\psi)\cdot\psi$ energy curves (which may not be the case for all porous materials). These curves increase linearly with suction from 0 to the AEV. As the hypothetical material presented here is qualified as "highly compressible", its porosity can decrease with increasing suction far beyond the AEV. However, it is worth mentioning that increasing $[E]_{cap}$ or $\chi(\psi)\cdot\psi$ does not necessarily mean that porosity decreases, because the energy may not be sufficient or adequate to cause shrinkage, particularly if the capillary stress is applied to the smallest pores.

It may be added that as the suction component of compression energy is null at complete desaturation, a rebound may be observed (although it was not yet observed in laboratory), similar to the one observed when mechanical stress is released from a soil sample submitted to an oedometer test.

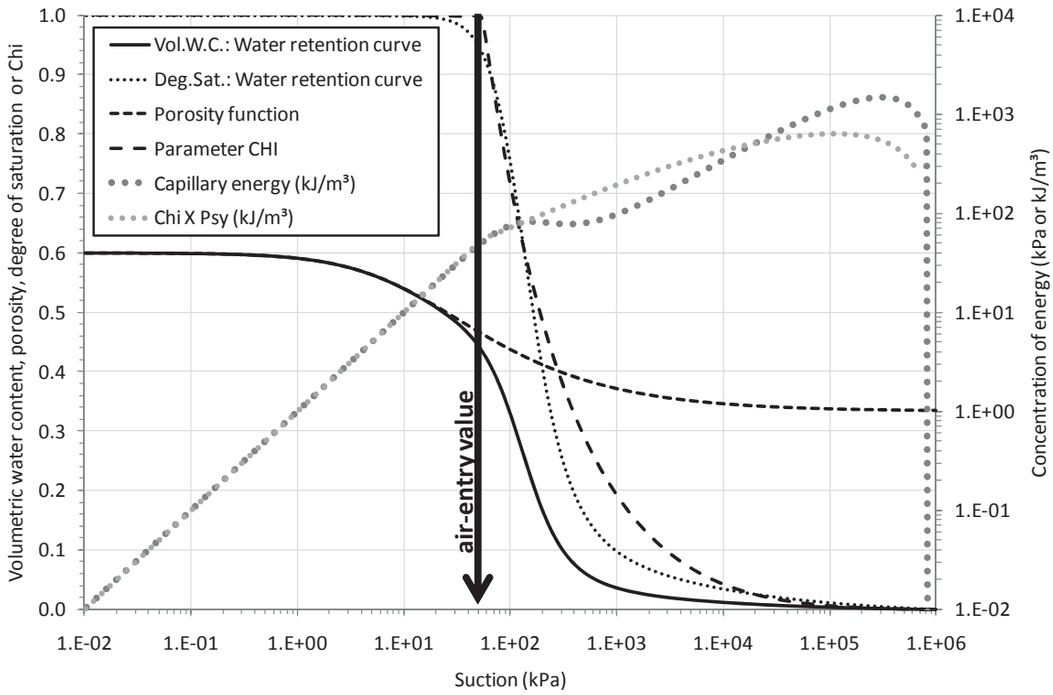


Fig. 3. The energy of compression conceptual approach and the variation of parameter χ

**2.1.2.2 Defining material compressibility with suction**

Any porous material is virtually compressible if it undergoes a sufficiently high level of stress. In the particular case of soils, the coefficient of compressibility is determined by consolidation tests and used for constitutive modeling (Roscoe & Burland, 1968). The compressibility is thus commonly regarded as a mechanical property characterizing the response of a material to an external, mechanical, stress. Yet, when describing the material response to suction changes, the term compressible material is not clearly defined in the literature. A clear definition is needed to proceed further. Using sensitivity of materials to suction, three categories were thus created:

- non compressible materials (NCM), e.g. ceramic, concrete;
- compressible materials (CM), e.g. sand, silt;
- highly compressible materials (HCM), e.g. fine-grained clays, peat, deinking by-products.

The definition considers a relationship between void ratio and gravimetric water content ($w$), commonly called the *soil shrinkage characteristic curve* (Tripathy, et al., 2002). However, because compressible porous materials are not necessary soils, this curve will be called *pore shrinkage characteristic curve* (PSCC) in this chapter.

Fig. 4 shows a schematic representation of three PSCCs. The NCM (coarse dashed line) does not shrink under the effect of suction. The CM (fine dashed line) shrinks only when it is saturated. Finally, the highly compressible material (solid line) shrinks over a range of suction that goes beyond the AEV (e.g. as shown by Kenedy & Price (2005) for peat). In other words, the capillary energy is not high enough to produce significant shrinkage to the NCM. The CM shrinks under suction, but the capillary energy is not high enough to

produce significant shrinkage at suction values higher than the AEV. As for HCM, the compression energy induced by capillary forces makes the pores shrink even for suction values beyond the AEV. The sigmoïdal effect represented on the HCM curve is due to an asymptotical tendency to reach the shrinking limit at high suction values, near complete desaturation (theoretically at a suction of $10^6$ kPa). This behavior is treated in the "results and discussion" section, hereafter.

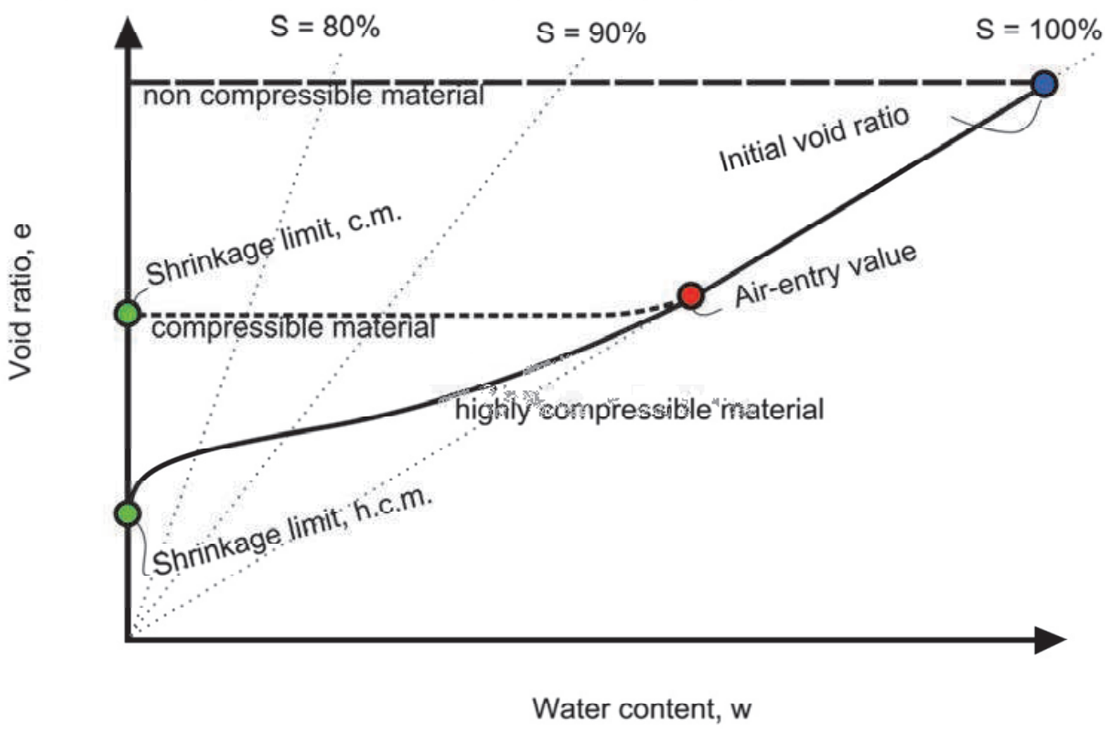


Fig. 4. Schematic representation for the definition of non compressible materials, compressible materials and highly compressible materials (S is degree of saturation)

### 2.2 The Water Retention Curve

The relationship between water content and suction in a porous material is commonly called the Water Retention Curve (WRC) and constitutes a basic relationship used in the prediction of the mechanical and hydraulic behaviors of unsaturated porous materials used in geotechnical and soil sciences. The theory associated with the prediction of the engineering behavior of unsaturated soils using the WRC is presented by Barbour (1998). Leong & Rahardjo (1997) summarize the equations to model the WRCs, mainly of the non-linear, fully reversible type. A review of recent models for WRC including capillary hysteresis, drying-wetting cycles, irreversibilities and material deformations is proposed by Nuth & Laloui (2008). Again, only the drying (desaturation) branch of the WRC will be studied here. Fig. 5 shows a schematic representation of a set of WRCs for the same material consolidated to different initial void ratios. It has been explained before that a porous material may shrinks while it dries. The various WRCs presented in terms of volumetric water content $\theta$ versus suction $\psi$ in Fig. 5 superimpose onto a single desaturation branch (solid thick line in

Fig. 5) for suction levels that are higher than the AEV ($\psi_{aev}$) of each single curve (Fredlund, 1967; Toll, 1988). This common desaturation branch is equivalent to the virgin consolidation of clayey soils. The AEV is a value of suction where significant water loss is observed in the largest pores of a specimen. As shown later, the AEV depends on the initial void ratio and on how the void ratio changes with suction. It is important to note that for HCMs, the AEV should be determined on a degree of saturation versus suction plot, rather than on the volumetric water content versus suction curve, because the volumetric water content of a sample can start to drop without emptying its pores. Indeed, if it is assumed that the volume of water expelled is equal to the decrease in void ratio, the volumetric water content decreases whereas the degree of saturation remains the same (Fig. 5).

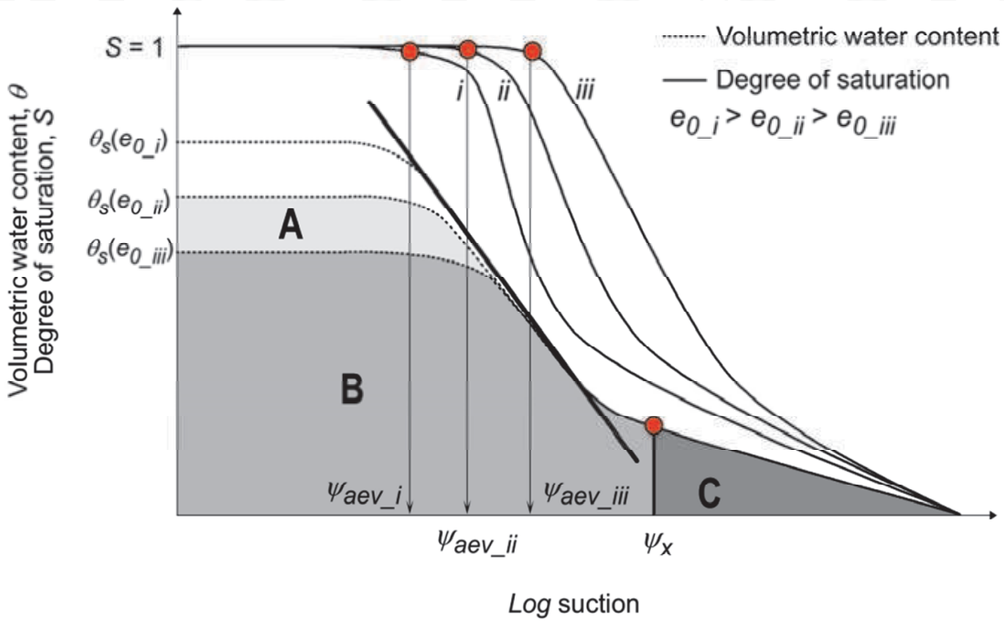


Fig. 5. Water retention curves for a material initially consolidated to different void ratios

The shape of the WRC is mainly influenced by the soil pore size distribution and by the compressibility of the material (Smith & Mullins, 2001). Pore size distribution and compressibility depend on initial water content, soil structure, mineralogy and stress history (Simms & Yanful, 2002; Vanapalli, et al., 1999; Lapierre, et al., 1990). Volume change (shrinkage) during desaturation can markedly influence the shape of the WRC. Emptying voids as suction increases may lead to a reduction in pore size, which in turn affects the estimated volumetric water content ($\theta$) and degree of saturation ($S$). Accordingly, taking into account volume change during suction testing is of great importance, be it in the laboratory or in the field, in order to avoid eventual flaws in the design of geoenvironmental and agricultural applications, be it a misinterpretation of strain, hydraulic conductivity or water retention (Price & Schlotzhauer, 1999). Cabral et al. (2004) proposed a testing apparatus based on the axis translation technique to measure volume change continuously during determination of the WRC of HCMs. This apparatus is presented in the "Materials and methods" section.

An extensive body of literature exists regarding the experimental determination of the WRC (Smith & Mullins, 2001). Although there are multiple procedures to determine WRCs, the volumetric water content of a HCM specimen cannot be accurately obtained from a single

test. Indirect methods based on grain size distribution (i.e. a measure of the pore size distribution) are also widely used to obtain WRCs (Aubertin, et al., 2003; Zhuang, et al., 2001; Arya & Paris, 1981). However, these methods are not suitable to fibrous materials, such as deinking by-products, and do not consider the reduction in pore size when suction increases (nor the distribution of this reduction among the pores).

In fact, most precursor models employed to fit WRC data have been developed assuming that the material would not be submitted to significant volume changes (Brooks & Corey, 1964; van Genuchten M. T., 1980; Fredlund & Xing, 1994). In particular, the WRC model proposed by Fredlund & Xing (1994) was elaborated based on the assumption that the shape of the WRC depends upon the pore size distribution of the porous material. The Fredlund & Xing (1994) model is expressed as follows:

$$\theta(\psi) = \frac{C(\psi)\theta_s}{ln\left(\exp(1) + \left(\frac{\psi}{a_{FX}}\right)^{n_{FX}}\right)^{m_{FX}}}$$

or (9)

$$S(\psi) = \frac{C(\psi)}{ln\left(\exp(1) + \left(\frac{\psi}{a_{FX}}\right)^{n_{FX}}\right)^{m_{FX}}}$$

where $\theta$ is the volumetric water content, $\theta_s$ is the saturated volumetric water content, $S$ is the degree of saturation, $\psi$ is the matric suction, $a_{FX}$ is a parameter whose value is directly proportional to the AEV, $n_{FX}$ is a parameter related to the desaturation slope of the WRC curve, $m_{FX}$ is a parameter related to the residual portion (tail end) of the curve, $C(\psi)$ is a correcting function used to force the WRC model to converge to a null water content at $10^6$ $kPa$ (Equation 10).

$$C(\psi) = 1 - \frac{ln\left(1 + \frac{\psi}{C_r}\right)}{ln\left(1 + \frac{10^6}{C_r}\right)} \tag{10}$$

where $C_r$ is a constant derived from the residual suction, i.e. the tendency to the null water content.

Huang et al. (1998) developed a WRC model that takes into account volume change in the mathematical definition of the WRC. Using experimental data reported in the literature, Huang et al. (1998) assumed, based on experimental evidence, that the logarithm of the AEV was directly proportional to the void ratio obtained at the AEV, as expressed as follows:

$$C(\psi) = 1 - \frac{ln\left(1 + \frac{\psi}{C_r}\right)}{ln\left(1 + \frac{10^6}{C_r}\right)} \tag{11}$$

$$\psi_{aev} = \psi_{aev_{e'}} 10^{\varepsilon_\psi (e - e')}$$

where $e$ is the void ratio, $e'$ is a reference void ratio, $\psi_{aev_{e'}}$ is the AEV at the reference void ratio $e'$, $\varepsilon_\psi$ is the slope of the $log(\psi_{aev})$ vs. $e$ curve, and $\psi_{aev}$ is the AEV at the void ratio $e$.
Later, Kawai et al. (2000) validated Huang et al. (1998)'s results. They also proposed that the void ratio at AEV would follow a curve that could be predicted from the initial void ratio defined by Equation 12. This equation was recovered in later studies, namely Salager et al. (2010) and Zhou & Yu (2005).

$$\psi_{aev} = Ae_0^{-B} \tag{12}$$

where $e_0$ is the void ratio at the beginning of the test, and A and B are fitting parameters.
Nuth & Laloui (2008) proposed a review of the published evidence of the dependency of the AEV with the void ratio and external stress for several materials, which also supports Equations 11 and 12.
An adaptation of the Brooks & Corey (1964) model was used by Huang et al. (1998) to describe the WRC of deformable unsaturated porous media, as follows:

$$S_e = \begin{cases} 1 & if \;\; \psi \leq \psi_{aev_{e\prime}} 10^{\varepsilon_\psi (e-e\prime)} \\ \left( \dfrac{\psi_{aev_{e\prime}} 10^{\varepsilon_\psi (e-e\prime)}}{\psi} \right)^{\lambda} & if \;\; \psi \geq \psi_{aev_{e\prime}} 10^{\varepsilon_\psi (e-e\prime)} \end{cases} \tag{13}$$

where $S_e$ is the normalized volumetric water content $[S_e = (S - S_r)/(1 - S_r)]$, $S_r$ is the residual degree of saturation, $\lambda$ is the pore size distribution index for a void ratio $e$, representing the slope of the desaturation part. Typical values for $\lambda$ range from 0.1 for clays to 0.6 for sands (van Genuchten, et al., 1991).
Shrinkage reduces the slope of the desaturation part of the WRC. Huang et al. (1998) assumed and provided evidence that, for HCMs, the relationship between $\lambda$ and void ratio can be represented by:

$$\lambda = \lambda_{e\prime} + d(e - e') \tag{14}$$

where $d$ is an experimental parameter and $\lambda_{e'}$ is the pore-size distribution index for the reference void ratio $e'$.
In other modeling frameworks published recently (Ng & Pang, 2000; Gallipoli, et al., 2003; Nuth & Laloui, 2008), the WRC model is coupled with a mechanical stress-strain model. Yet the calibration of these models requires an exhaustive characterization of the mechanical behavior which is not always available in the case of landfills, and out of the scope of this chapter.
It is relevant to note that the Huang et al. (1998) model does not model shrinkage as a function of suction and the partial desaturation for suctions lower than the AEV. A model designed to fit water retention data of a highly compressible material, presented in the results and discussion section, fulfill these gaps.

### 2.3 The hydraulic conductivity function

The hydraulic conductivity function (*k*-function) of unsaturated soils can be determined directly, by means of laboratory (McCartney & Zornberg, 2005; DelAvanzi, 2004) or field

testing, or indirectly, by empirical, macroscopic or statistical models. Leong & Rahardjo (1997) summarized current models used to determine the *k*-functions from WRCs. Huang et al. (1998) proposed to take into account the variation in $k_{sat}$ with *e* in the *k*-function model, as well as a linear variation in $log(k_{sat})$ with *e*.

$$k(e) = k_{sat}(e) \cdot k_r(\psi)$$
$$k_{sat}(e) = k_{sat_{e'}} 10^{b(e-e')} \tag{15}$$

where $k(e)$ is the hydraulic conductivity, $k_{sat}(e)$ is the saturated hydraulic conductivity at void ratio $e$ , $k_r(\psi)$ is the relative *k*-function that can be described using a model such as Fredlund et al. (1994) (Equation 16 below), $k_{sat_{e'}}$ is the saturated hydraulic conductivity at the reference void ratio $e'$ and $b$ is the slope of the $log(k_{sat})$ versus $e$ relationship. The relative *k*-function, $k_r$, and the void ratio, $e$, can be a function of either $\theta$ or $\psi$.

Since, for HCM, void ratio is a direct function of suction (Khalili, et al., 2004), it is convenient to use a *k*-function model integrated along the suction axis, i.e. $k_r(\psi)$. The relative *k*-function statistical model proposed by Fredlund et al. (1994), adapted from Child & Collis-George (1950)'s model, is expressed as follows:

$$k_r(\psi) = \frac{\int_{ln(\psi)}^{ln(10^6)} \frac{\theta\big(exp(y)\big) - \theta(\psi)}{exp(y)} \theta'\big(exp(y)\big) dy}{\int_{ln(1)}^{ln(10^6)} \frac{\theta\big(exp(y)\big) - \theta_s}{exp(y)} \theta'\big(exp(y)\big) dy} \tag{16}$$

where $\theta$ is the first derivative of the WRC model and $y$ is a dummy integration variable representing suction.

It is important to note that, as mentioned by Fredlund & Rahardjo (1993), the Child & Collis-George (1950)'s *k*-function model, from which Equation 15 and Equation 16 were derived, assumed incompressible soil structure. In fact, the function on the numerator in Equation 16 was integrated from suction value $ln(\psi)$ to the maximum suction value, $ln(10^6)$, while the denominator was computed over the entire suction range, *i.e.* from $ln(0)$ (where $\exp(ln(0)) \rightarrow 0$) to $ln(10^6)$. However, the function on the denominator is not the same for two porous materials with different initial void ratios, with different initial $\theta_s$. Consider samples *ii* and *iii* in Fig. 5, the schematic representation of three water retention tests performed with different initial void ratios. It was expected that at suction $\psi_x$, samples *ii* and *iii* would reach the same void ratio, the same volumetric water content and, as a result, the same hydraulic conductivity. However, considering that the function to integrate is a function of WRC, the denominator of Equation 16 must be larger if calculated over the function derived from the WRC of sample *ii* (areas A+B+C, Fig. 5) then compared to sample *iii* (areas B+C, Fig. 5), leading to different *k*-functions.

Theoretical explorations can be derived for from better understandings of the mechanism of capillary-induced shrinkage. Such exploration was performed by Parent & Cabral (2004), who proposed means to estimate the *k*-function of an HCM from water retention tests over the saturated range. This method is presented in the "Results and interpretation" section.

### 2.4 Synthesis of the theory section

The mechanistic model presented herein is coherent with Bishop (1959)'s empirical model (Equation 2): $\psi \cdot \chi$ is null at 0 and $10^6$ *kPa* and a maximum is observed. The compression energy concept offers a mechanistic perspective that leads to a better understanding. This new paradigm led the authors to three arguments:

1. regarding to suction, definitions can be formulated for non compressible, compressible and highly compressible materials;
2. parameter $\chi$ can be used in several manners to deduce the compression behavior of a porous material;
3. water retention curve and *k*-function models that takes into account volume compression of a porous material when drying needs may be needed.

## 3. Materials and methods

The materials used in this study, as well as the methods used to determine their properties, are presented in this section. An experimental protocol for the measurement of the water retention curve (WRC) of highly compressible materials (HCMs) is detailed.

### 3.1 Determination of the water retention curve of deinking by-products

#### 3.1.1 Deinking by-products

Deinking by-products (DBP), also known as fiber-clay, are a fibrous and highly compressible paper recycling by-products composed mainly of cellulose fibers, clay and calcite (Panarotto, et al., 2005) (Fig. 6). The composition of DBP varies significantly with the type of paper recycled and the efficiency of the deinking process employed (Latva-Somppi, et al., 1994). DBP was characterized in the scope of many works (Panarotto, et al., 2005; Cabral, et al., 1999; Panarotto C., et al., 1999; Kraus, et al., 1997; Vlyssides & Economides, 1997; Moo-Young & Zimmie, 1996; Latva-Somppi, et al., 1994; Ettala, 1993). DBP leaves the production plant with gravimetric water content varying from 100% to 190% (Panarotto, et al., 2005). The maximum dry unit weight obtained using the Standard Proctor procedure ranges from 5.0 to 5.6 kN/m$^3$. The optimum gravimetric water content ranges from 60 to 90%. Fig. 7 presents the consolidation over time of DBP specimens in the laboratory as well as in the field. The field data collected from three sectors of the Clinton mine cover, Quebec, Canada, presented in Figure 7 illustrates the time-dependent nature of the settlements of the DBP and reveals a short primary consolidation phase during the first two months, followed by a long secondary consolidation (creep) phase. Hydraulic conductivity tests were performed in oedometers at the end of each consolidation step in the laboratory. The results are presented in Fig. 8, which shows the saturated hydraulic conductivity obtained for a series of tests performed with samples collected from different sites and prepared at an average initial gravimetric water content of approximately 138% (approximately 60% above the optimum water content). As expected, the saturated hydraulic conductivity increased with increasing void ratio, defining a slope of the mean linear relationship. The parameter *b*, i.e. the slope of the *e* versus $log(k)$ linear relationship in Equation 15, equals 0.95. Although the influence of the extreme bottom-left point is minor in the curve-fitting procedure, it may infer that the *e* versus $log(k)$ relation would be exponential rather than linear. Such relations were obtained by Bloemen (1983) for peat soils. However, in the case presented here, more points would be needed in the $10^{-10}$ m/s order of magnitude to conclude on the existence of such curved relation.

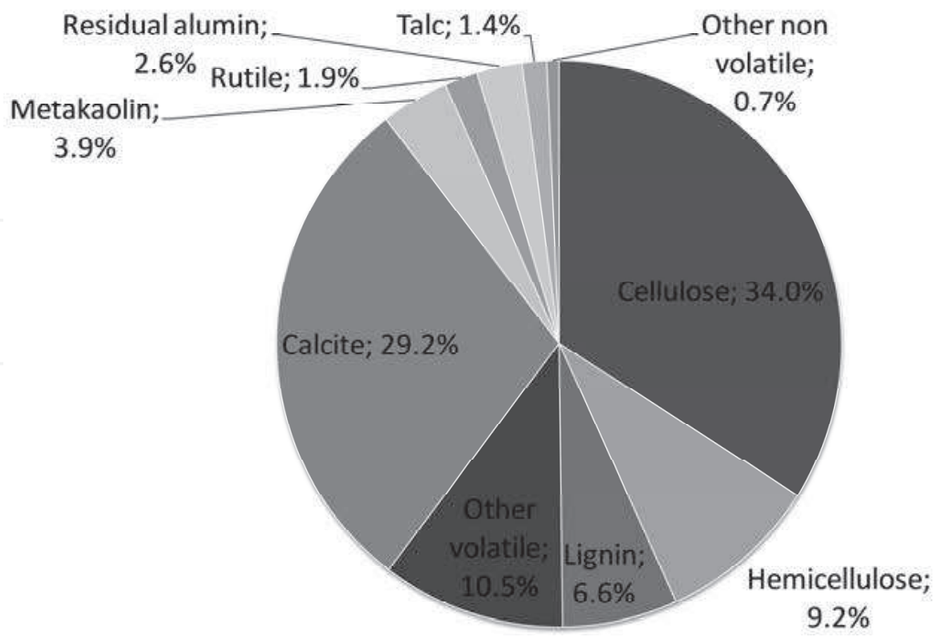


Fig. 6. Average composition of the DBP used in the experimental program (% by weight), adapted from (Panarotto, et al., 2005)

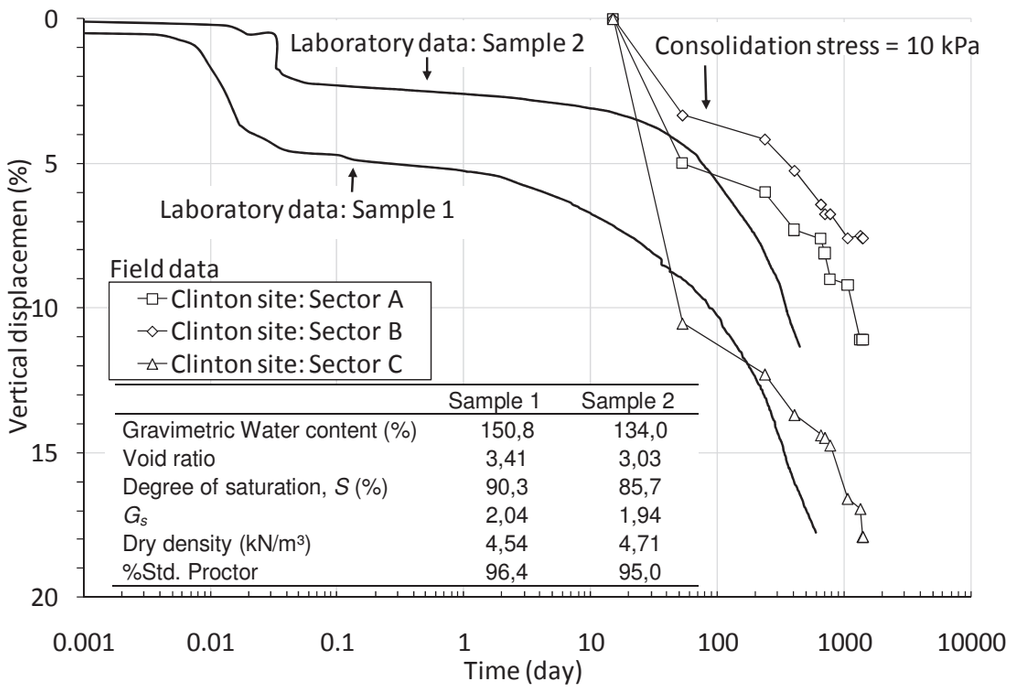


| | Sample 1 | Sample 2 |
|---|---|---|
| Gravimetric Water content (%) | 150,8 | 134,0 |
| Void ratio | 3,41 | 3,03 |
| Degree of saturation, *S* (%) | 90,3 | 85,7 |
| $G_s$ | 2,04 | 1,94 |
| Dry density (kN/m³) | 4,54 | 4,71 |
| %Std. Proctor | 96,4 | 95,0 |

Fig. 7. Typical consolidation behaviour of deinking by-products from laboratory testing and from field monitoring of three sites (adapted from Burnotte et al. (2000) and Audet et al. (2002))

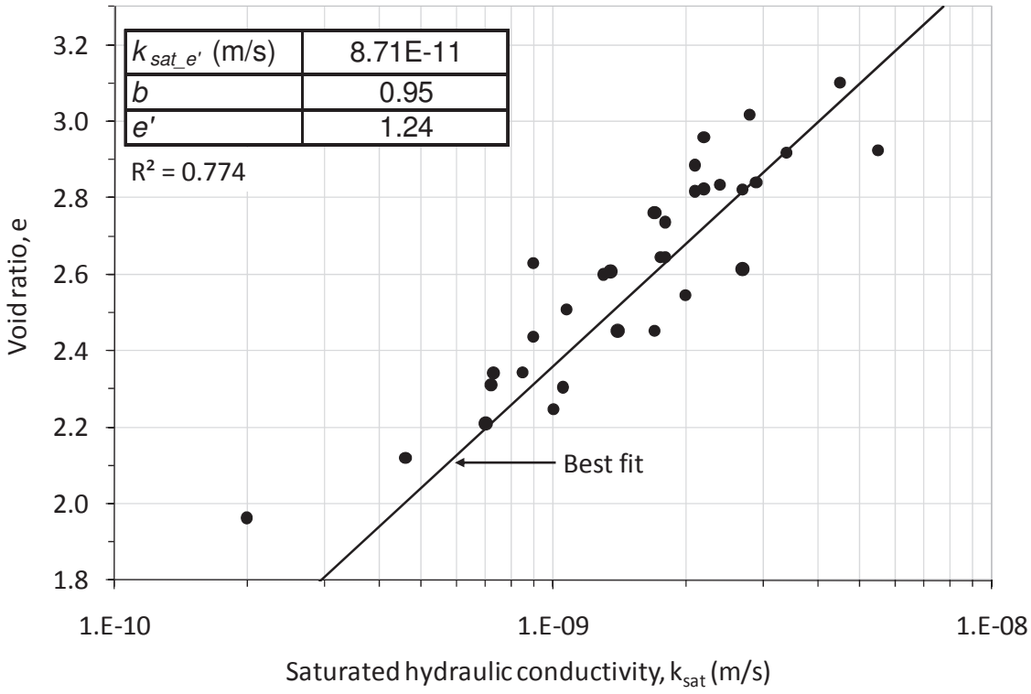


Fig. 8. Void ratio as a function of saturated hydraulic conductivity for deinking by-products

### 3.1.2 Testing equipment to determine the water retention curve

#### 3.1.2.1 Pressure plate drying test (modified cell test) with continuous measurement of volume changes

Fig. 9 shows a schematic view of the testing apparatus used in this study to obtain the water retention curve (WRC) of DBP. A picture of the apparatus is shown in Fig. 10. The system consists of a 115.4−mm high, 158.5−mm diameter acrylic cell, a pressure regulator to control air pressure applied to the top of the sample and to the burette "CELL", and three valves to control air pressure, water inflow and water outflow. As the air pressure applied on the top of the specimen is increased, water is expelled from the sample and collected in burette "OUT". Any change in volume of the specimen during pressure application results in an equivalent volume of water that enters the cell via the burette CELL. The apparatus thus allows continuous measurement of volume changes, allowing the calculation of volumetric water content at each suction level. Further details of the equipment and testing protocol are described in Cabral et al. (2004).

Cabral et al. (2004) used a porous stone with negligible air-entry value (AEV, 0−*bar* porous stone). However, as suction increased beyond the AEV of DBP, air entering the DBP specimen drained the porous stone. In the present study, testing was performed using porous stones with AEVs of 1 *bar* or 5 *bar* (1 *bar* = 101.3 kPa). The use of a 1−*bar* or 5−*bar* porous stone allowed WRC data to be obtained up to suction values of 100 kPa or 500 kPa, respectively. The time needed to reach equilibrium in burettes OUT and CELL after each pressure increment was carefully evaluated. Consistent readings could be made every 24 hours with the 0−*bar* porous stone and after 2 to 5 days for 1−*bar* and 5−*bar* porous stones, depending on the level of pressure applied.

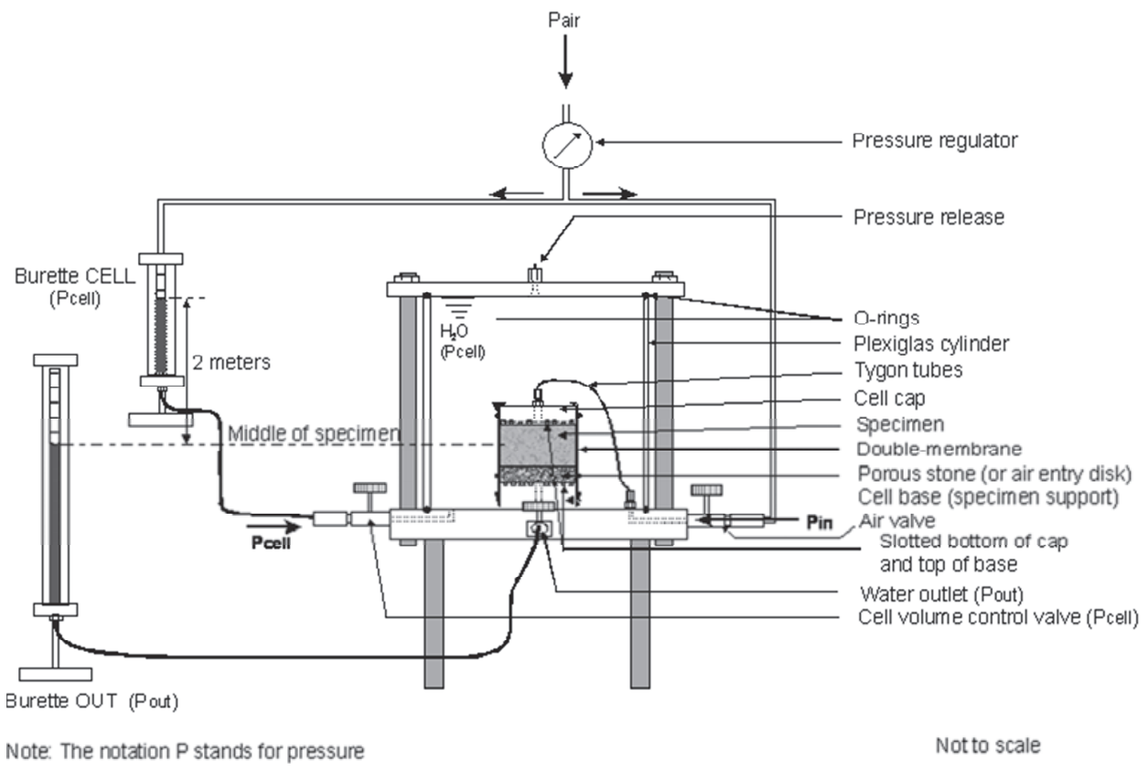


Fig. 9. Scheme of the testing system developed at the Université de Sherbrooke

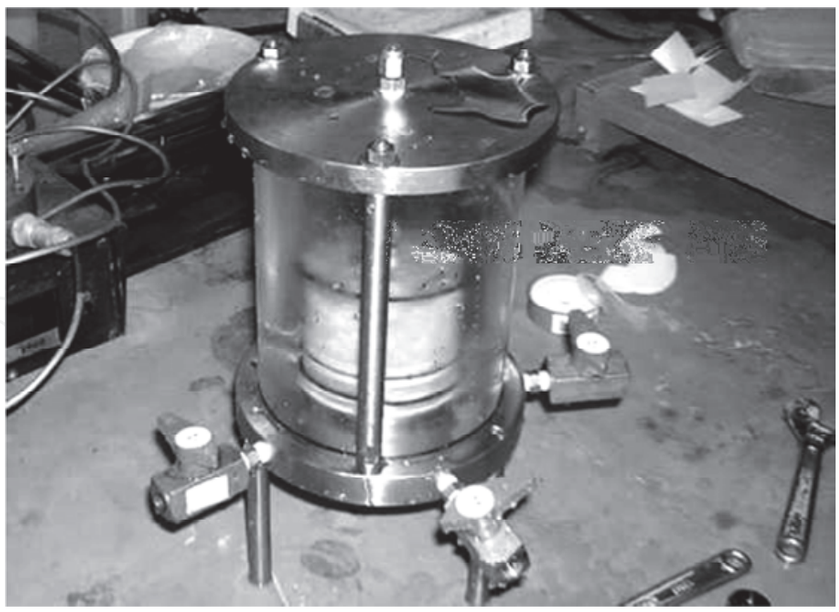

Fig. 10. Picture of the testing system developed at the Université de Sherbrooke

***3.1.2.1.1 Sample preparation***

A mass of about 20 kg of DBP was sampled from a pile. From this sample, about 1 kg per test was sampled for the four tests presented in this chapter. Rare gravel particles were

removed. Initial autoclaving of the materials at 110°*C* and 0.5 *bars* is required to prevent biological activity during testing. Planchet (2001) observed that the use of microbiocide changed the pore structure of DBP by alterating the fibers. Consequently, only autoclaving was performed to prevent microbes to grow into the DBP specimens.
Preliminary tests with DBP showed that the procedure leading to the best reproducibility required compacting three 10 *mm*-thick layers of material by tamping DBP material directly into the cell. For that purpose, a mould and small mortar were designed and constructed (Fig. 11a). The thickness of the layers was controlled using a specially designed piston (Fig. 11b). The initial void ratio of a test was controlled by determining the mass of sample needed to be compacted in each layer. Cabral et al. (2004) provide further details of the procedure for sample preparation and compaction. The characteristics of the samples of DBP used in this study, modified cell tests (MCT) 1 to 4, are presented in Table 2. The data were calculated from the mass of humid material constituting the sample, water content test in a non ventilated oven at 110°*C*. The relative density was determined thanks to a volumetric method grain density test.

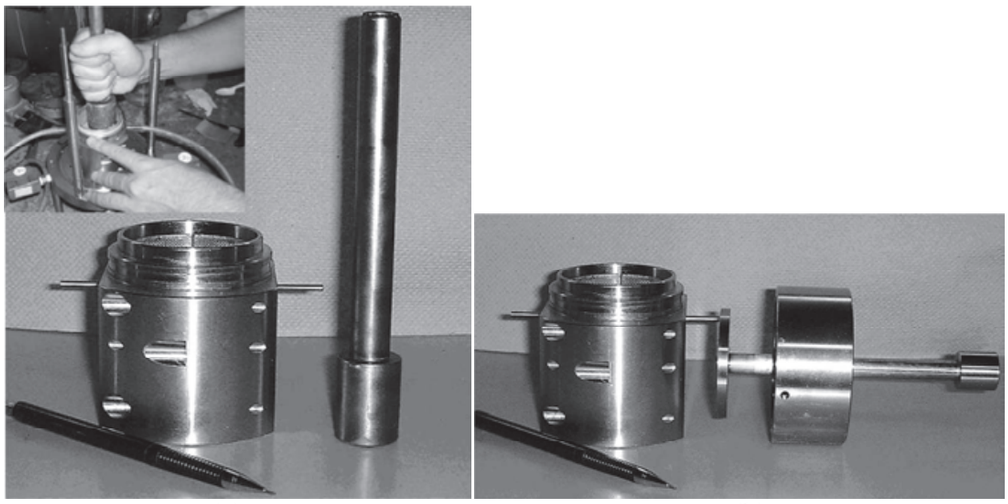

(a) (b)

Fig. 11. Tools used for the modified cell test sample preparation: (a) mould and mortar (b) mould and piston

| | MCT1 | MCT2 | MCT3 | MCT4 |
|---|---|---|---|---|
| **Gravimetric water content (%)** | 196.9 | 153.6 | 210.3 | 188.5 |
| **Unit weight (*kN/m*³)** | 11.76 | 11.58 | 11.25 | 11.72 |
| **Degree of saturation (%)** | 99.4 | 93.3 | 99.9 | 99.1 |
| **Relative density** | 1.99 | 1.99 | 1.99 | 1.99 |
| **Initial void ratio** | 3.89 | 3.28 | 3.67 | 2.70 |
| **Porous stone used for the test** | 1−*bar* | 1−*bar* | 1−*bar* | 5−*bar* |

Table 2. Characteristics of four specimens tested into the modified cell (MCT) in this study (evaluated after compaction directly into the mold and before the test assembly)

***3.1.2.1.2 Testing and calibration***

Following compaction, the apparatus was assembled and the consolidation phase initiated. Consolidation was conducted during 120 minutes under a cell confining pressure of 5 kPa.

The valve allowing air into the sample remained closed during this adjustment phase. The pressure was then raised to 20 kPa for a second consolidation phase that lasted 24 hours. A pressure of 20 kPa corresponded approximately to the overburden pressure applied by the protection cover layers to a barrier layer of DBP.

The first point of the WRC was taken at the end of the consolidation phase under 20 kPa, which occurred when the water levels in the burettes CELL and OUT reached equilibrium. At this point, readings were initialized and air pressure increments of 2.5 kPa (irregular increments for MCT4) were applied to the specimen until reaching the suction corresponding to the AEV as clearly identified on the $\psi$ vs. $\theta$ plot. Pressure increments of 10 kPa were then applied at suction levels higher than the AEV (irregular increments for MCT4).

The volume of water entering the cell (from burette CELL), corresponding to changes in specimen volume, was recorded during each pressure increment. The water volume reaching the burette OUT was also recorded to indicate the volume of water lost from the MCT specimen. Calibration of the system was conducted to account for the expansion of the cell and the lines. Details of the calibration procedure are provided by Cabral et al. (2004). After appropriate corrections were applied to the recorded values, the water content and degree of saturation of the specimen is determined for the applied air pressure level. Since the axis translation technique was employed, the air pressure corresponded to the suction in the specimen. Stabilization of volumetric water content was reached when two consecutive measurements, taken 24 h apart, show a difference of less than 0.25% in water content for MCT1 to MCT3 and 0.5% for MCT4.

Tests were ended when suction reached the AEV of the porous stone. The cell was then disassembled and the final dimensions and weight of the sample were recorded.

HCMs have usually highly hysteretic behavior, which would affect water retention and flow. In this study, only desaturation was tested. The reader looking for more information about the hysteresis phenomenon on HCMs may refer to Nuth & Laloui (2008).

## 4. Results and interpretation

This chapter contains mathematical models developed to estimate the hydraulic properties of highly compressible materials (HCM).

### 4.1 Hydraulic properties of highly compressible materials

This section presents a water retention curve (WRC) model developed from the results of an experimental program performed to determine the WRC of deinking by-products (DBP). This model is able to fit several water retention curves of highly compressible materials using a single set of parameters and is validated using published data. The hydraulic conductivity function (*k*-function) was derived from the WRC proposed model using Fredlund et al. (1994)'s model (Equation 16). Moreover, a model to predict the *k*-function of HCM based on tests with saturated sample is presented and compared to results using Fredlund et al. (1994)'s model.

#### 4.1.1 Results of the experimental program

The results obtained in the experimentation phase of this research program are interpreted in this section, leading to two models:

- a model to fit WRC data of a HCM;
- a model to predict the *k*-function of a highly compressible material (HCM) based on tests with saturated samples.

The first is an adaptation of a common WRC model (Fredlund & Xing, 1994) considering suction-induce consolidation curve. The second is an alternative procedure based on two relationships: void ratio versus saturated hydraulic conductivity and void ratio at the air-entry value (AEV) versus AEV.

#### 4.1.1.1 Model to fit water retention data of a highly compressible material

If porous materials whose void ratios converge toward the same value under increasing suction application, irrespective of their initial void ratio (Fig. 5), it can be expected that, at a certain suction value, the parameters governing the shape of the WRC should reach the same values. Accordingly, the model proposed herein, which is based on the Fredlund & Xing (1994) WRC model, is able to describe multiple WRC test results for the same HCM with different initial void ratios using a single set of parameters. The adaptation consists in the variation of the four parameters of the Fredlund & Xing (1994) model ($a_{FX}$, $n_{FX}$, $m_{FX}$ and $\theta_s$) with void ratio. In this section, a void ratio function model, a WRC model and a hydraulic conductivity function ($k$-function) model are presented.

Rode (1990) approximated the effect of hysteresis and found that the effect on the calculated water content was not large. However, investigations performed by Price & Schlotzhauer (1999) showed that the shrinkage behavior of peat, a material with high organic content like DBP, was highly hysteretic. Nevertheless, this aspect is not covered in the present study. Considering hysteresis would lead to the prediction of lower water content and hydraulic conductivity values for a same suction value.

##### *4.1.1.1.1 The water retention curve model*

For HCMs, a gradual desaturation takes place before the AEV is reached, as shown for peat by Weiss et al. (1998), Schlotzhauer & Price (1999) and Brandyk et al. (2003), and for DBP by Cabral et al. (2004). Therefore, the two-phase behavior of Huang et al. (1998)'s model (Equation 13) may lead to a model bias. The Fredlund & Xing (1994) model (Equation 9) was adapted in this study to account for volume changes, including the region where suction is lower than the AEV.

Fig. 12 shows the relationship between $log(\psi_{aev})$ and $e_{aev}$ obtained from suction tests performed using DBP (MCT1 to MCT4 and tests 15 and 16 from Cabral et al. (2004)). Parameters of Equation 11 obtained from $R^2$ maximization over the data are shown in Table 3. In the cases where a 0-*bar* porous stone was employed (tests 15 and 16), AEV was considered to be equal to the suction value where air broke through the sample (which is an approximation). In the cases where 1-*bar* or 5-*bar* porous stones were employed (MCT1 to 4), the AEV was considered to be equal to the suction value where significant loss of water was observed on the $S$ versus $\psi$ curve. The relationship between $log(\psi_{aev})$ and $e_{aev}$ is approximately linear and can be described using Equation 11. According to Fredlund et al. (2002), the parameter $a_{FX}$ defines the lateral position of the WRC and is linearly proportional to AEV. Consequently, for HCM, the variation of $a_{FX}$ with void ratio can be stated to be similar to the variation of $\psi_{aev}$, as in Equation 17. This model was preferred over Kawai et al. (2000)'s model (Equation 12), being more closely related to experimental.

$$a_{FX} = a_{FXe'} 10^{\varepsilon_a (e - e')} \tag{17}$$

where $a_{FXe'}$ is the value of $a_{FX}$ at a reference void ratio $e'$ and $\epsilon_a$ is the slope of the $log(a_{FX})$ and $e_{aev}$ curve. In order to reduce the number of parameters, the value of $e$ can be set to $e_c$. For $e = e_c$, the more compressible the material is, the closer $a_{FXe'}$ will be from residual suction ($C_r$). Moreover, since $a_{FX} \propto \psi_{aev}$, $\varepsilon_a = \varepsilon_\psi$.

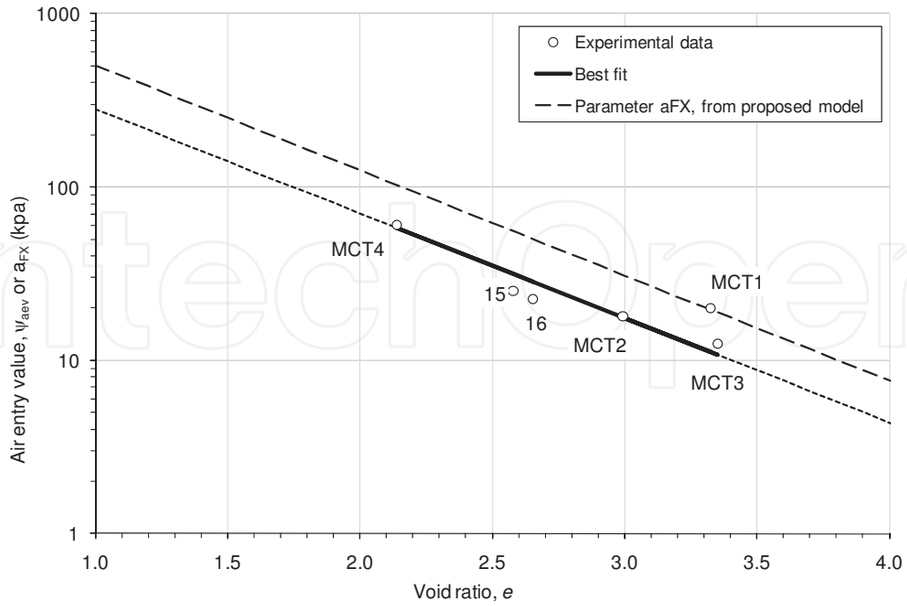


Fig. 12. Air-entry value as a function of void ratio at the air-entry value

| | |
|---|---|
| $\psi_{aev\_e'}$ | 731 |
| $\varepsilon_{\psi}$ | -0.603 |
| $e'$ | 0.31 |
| $R^2$ | 0.891 |

Table 3. Parameters of Equation 11 obtained from $R^2$ maximization over MCT1 to MCT4 and tests 15 and 16 from Cabral et al. (2004)

In the Huang et al. (1998) model, the parameter $\lambda$ is assumed to vary linearly with $e$. In the proposed model, the same assumption is made concerning the parameters $n_{FX}$ and $m_{FX}$ (Equation 9), whose variation with void ration are described as follows:

$$n_{FX} = n_{FXe'} + \varepsilon_n(e - e') \tag{18}$$

$$m_{FX} = m_{FXe'} + \varepsilon_m(e - e') \tag{19}$$

where $n_{FXe'}$ and $m_{FXe'}$ are respectively the Fredlund & Xing (1994) parameters $n_{FX}$ and $m_{FX}$ at the reference void ratio $e'$, $\varepsilon_n$ and $\varepsilon_m$ are regression parameters obtained by least square minimization of WRC data. Note that the slope of the WRC tends to be null when $n_{FX}$, tends to unity (and void ratio tends to its suction-induced shrinkage limit).

#### *4.1.1.1.2 The void ratio function*

Fig. 13 shows pore-shrinkage characteristic curve (PSCC, i.e. void ratio versus water content) data from suction tests with DBP performed in order to obtain the WRC (tests MCT1 to MCT4), using the procedure described in the Materials and Methods section. The initial void ratio of the four tests ranged between 2.70 and 3.89 (Table 2.). The creep phases occurring for values lower than AEVs for every tests indicate that DBP is a HCM.

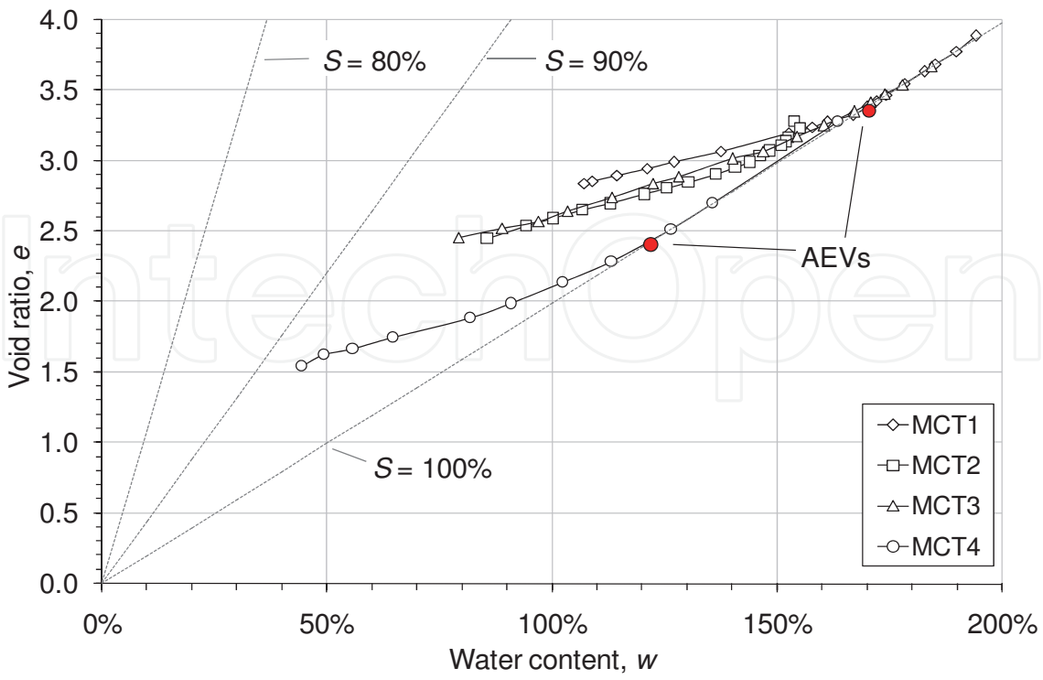


Fig. 13. Void ratio versus water content for deinking by-products under suction plus a total stress of 20 kPa

A void ration function (*e*-function) must be defined in order to estimate the variation of Fredlund & Xing (1994) model's parameters. Suction induced in a porous material is a stress that may result in pore shrinkage. Fig. 14 presents void ratio versus suction for four representative modified cell tests with DBP (MCT1 to 4). A total stress of 20 *kPa* was applied for all tests and several increments of suction were imposed. These results are compared to oedometer tests (thick line in Fig. 14). In the range of effective stresses applied in these tests, the exponential shape of the consolidation curve follows the same pattern as the suction induced consolidation behavior. However, the comparison has no quantitative value due to the fact that the axial stress measured in oedometer tests cannot be compared to the volumetric (mean) stress measured in desaturation tests.

Based on results for compressible soils, Huang et al. (1998) assumed that changes in void ratio occurred only for values of matric suction less than the AEV. However, the results obtained from tests MCT1 to 4, presented in Fig. 14, indicate that the above-mentioned assumption does not apply to HCMs such as DBP. Indeed, the void ratio continued to decrease significantly as suction increased, even for suction levels greater than the AEV. Salager et al. (2010) proposed and equation to link void ratio and suction. However, their model was not suitable to adequately fit our data, namely because it was not meant to consider the convergence of several tests to a unique shrinkage limit. The alternative exponential model in Equation 20, adapted from Ratkowski (1990), is proposed to describe the variation of void ratio as a function of suction as follows:

$$e_i = e_c + (e_{oi} - e_c)(1 + c_1 e_{oi}\sigma')^{c_2} \tag{20}$$

where $e_i$ is the void ratio at effective stress $\sigma'$ for test $i$, $e_{0i}$ is the void ratio in the beginning of the suction test $i$, and $c_1$, $c_2$ and $e_c$ are fitting parameters. The parameter $e_c$ is the void ratio at which the $e$ vs. $\sigma'$ curves obtained from compression or consolidation tests conducted using

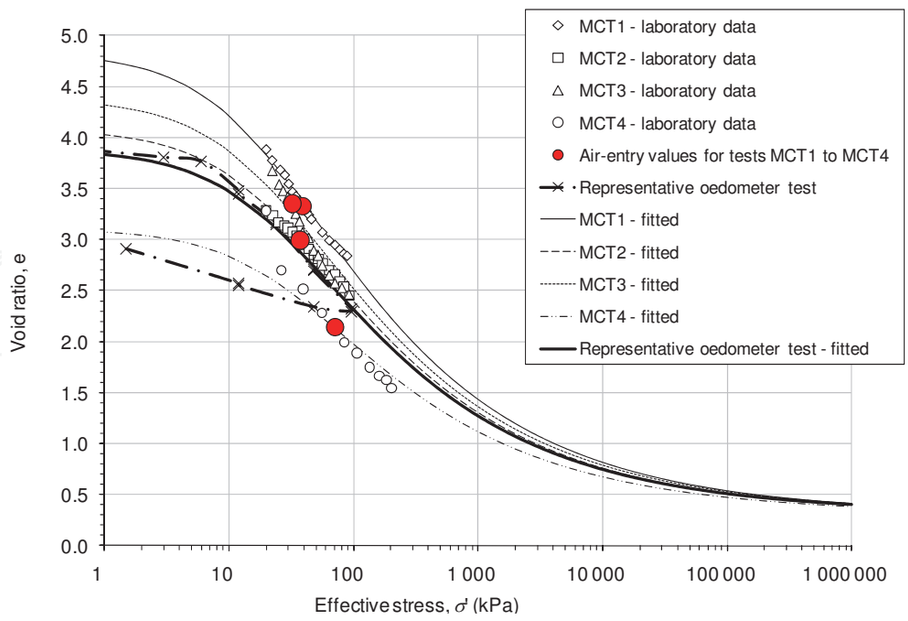


(a)

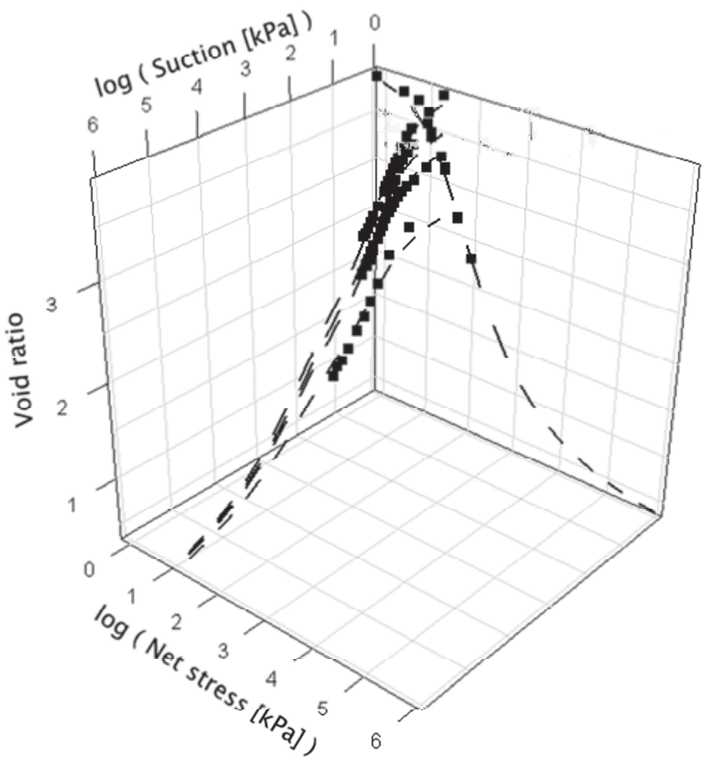


(b)

Fig. 14. (a) Void ratio versus effective stress $\sigma' = \sigma + S(\psi)\psi$ the effective stress is the axial one in the case of the oedometer Test) and (b) decomposed versus suction and net stress for four MCTs and one representative oedometer test

specimens prepared at different initial void ratios converge, the parameters $c_1$, $c_2$ and $e_c$ for DBP were obtained by a least square optimization technique (their values are presented in Table 4.), $\sigma$ is total (mechanical) stress and $\psi_{e_c}$ is the suction observed in the vicinity of $e_c$. The effective stress is defined in Equation 6, i.e. $\sigma' = \sigma + S(\psi)\psi$, where $S(\psi)$ is the WRC.
Fig. 3 shows that the suction component of compression energy may theoretically drop to zero at complete desaturation. Accordingly, although not observed yet in laboratory, a rebound should be observed, similar to the one observed when mechanical stress is released from a soil sample submitted to an oedometer test. This rebound is not described by the void-ratio function of Equation 20. The apparatus did not allow suction values higher than 500 kPa. Nevertheless, the *e*-function is of Equation 20 is an exponential function where two curves with different $e_{0i}$ values converge to a threshold value of $e_c$. Such convergence observed by Boivin et al. (2006) gives confidence in the assumption that the convergence towards an asymptotic void ratio value is still valid for suction values higher than 500 kPa. The *e*-function regression of Equation 20 was fitted to MCT and oedometer data by maximizing $R^2$. The parameters are shown in Table 4.

| | MCT1 | MCT2 | MCT3 | MCT4 | Oedometer |
|---|---|---|---|---|---|
| $e_0$ | 4.84 | 4.09 | 4.38 | 3.11 | 3.88 |
| $e_c$ | 0.31 | | | | |
| $c_1$ | 0.01097 | | | | |
| $c_2$ | -0.349 | | | | |
| $R^2$ | 0.980 | | | | |

Table 4. Parameters of the e-function for tests MCT1 to 4 and PPCT1 to PPCT4

The proposed WRC model (Equation 21) is then obtained by inserting Equation 20 into equations Equation 17 to Equation 19, and inserting Equation 17 to Equation 19 into Equation 9, with $e' = e_c$:

$$S(\sigma, \psi) = \frac{\left(1 - \frac{ln\left(1 + \frac{\psi}{C_r}\right)}{ln\left(1 + \frac{10^6}{C_r}\right)}\right)}{ln\left(exp(1) - \left(\frac{\psi}{A}\right)^B\right)^C} \tag{21}$$

Where

$$A = a_{FXe'} 10^{(e_{0i} - e_c)\left(1 + c_1 e_{0i}(\sigma + S(\psi)\psi)\right)^{c_2}}$$

$$B = n_{FXe'} + \epsilon_n (e_{0i} - e_c)\left(1 + c_1 e_{0i}(\sigma + S(\sigma, \psi)\psi)\right)^{c_2}$$

$$C = m_{FXe'} + \epsilon_m (e_{0i} - e_c)\left(1 + c_1 e_{0i}(\sigma + S(\sigma, \psi)\psi)\right)^{c_2}$$

The degree of saturation in Equation 21 is present on both sides of the equation, and its isolation is not possible. The proposed strategy is to evaluate a single $S(\sigma,\psi)$ based on a WRC function (Fredlund & Xing, 1994; Brooks & Corey, 1964; van Genuchten M. T., 1980) representing a whole data set and insert that function on the right-wing side of Equation 21.

The proposed WRC model is supported by a documented theoretical framework that supposes that it can be applied to most HCMs. The next section presents a validation procedure on a compressible silty sand.

#### *4.1.1.1.3 Validation of the proposed model*

In order to validate the proposed model (Equation 21), the procedure for obtaining the WRC and predicting the *k*-function was applied to experimental data published by Huang (1994) for a series of tests with a compressible silty sand from Saskatchewan, Canada. These tests were performed using pressure-plate cells. Changes in volume during testing were not recorded. As a consequence, the variation of void ratio with suction had to be derived from the results of flexible-wall permeability tests performed by Huang (1994) with specimens with similar initial void ratios.

In order to apply the proposed model, it is supposed that the silty sand behaves like a CM, i.e. void ratio converges toward a single value (the shrinkage limit). The proposed model was applied to fit the results of suction test data for specimens PPCT13, PPCT16 and PPCT22, taken from Huang et al. (1998). The parameter $a_{FX}$ was obtained using a $log(a_{FX})$ and $e_{aev}$ curve, where the AEV is determined on the $S$ versus $\psi$ curve. Fig. 15 shows the results of Huang et al. (1998) fitted with the proposed model. It can be observed that, using a single set of parameters, the proposed model superimposes the experimental results ($R^2$ = 0.978) rather well. At a value of about 700 *kPa*, the three curves practically merge into a same desaturation curve. The data ranged between 0 and 300 *kPa*. The predicted degrees of saturation corresponding to suction values higher than 300 *kPa* are extrapolated to reach a null value at a suction value of $10^6$ *kPa*.

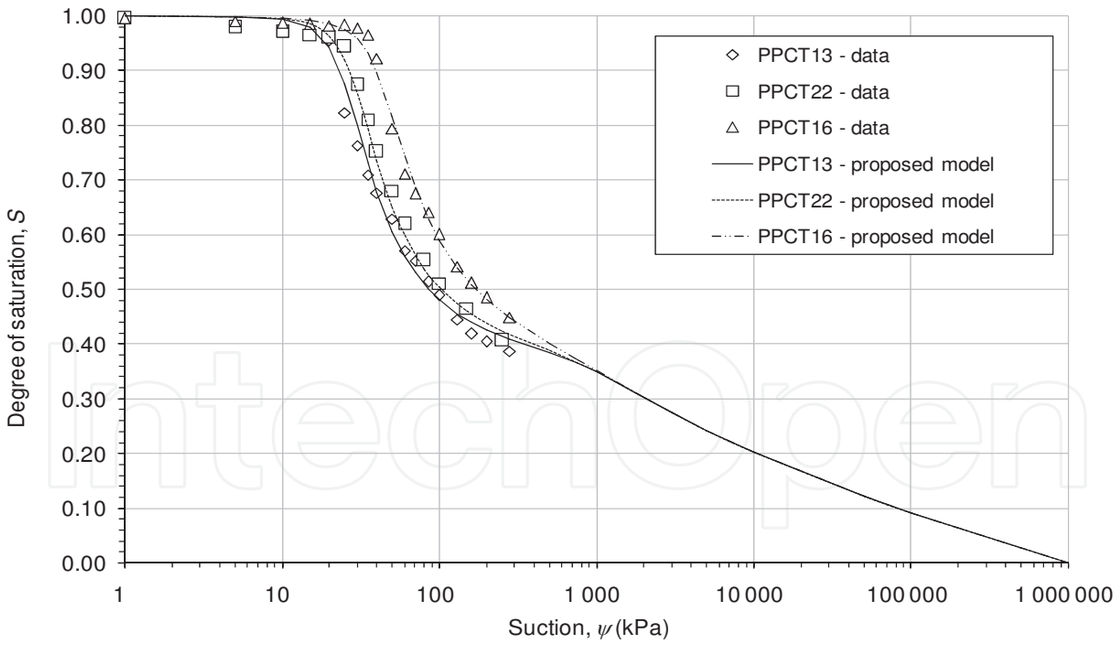


Fig. 15. Proposed water retention curve model to represent desaturation of a silty sand — data from Huang (1994)

Fig. 15 presents the results of three flexible-wall unsaturated hydraulic conductivity tests (FWPT2, FWPT3 and FWPT6) performed by Huang (1994) with the same Saskatchewan silty sand. These tests were chosen because their initial void ratios are similar to those of PPCT13,

PPCT22 and PPCT16, respectively. Parameter of the e-function and of the proposed WRC, shown inTable 5, were obtained by maximizing $R^2$.

| | PPCT13 | PPCT22 | PPCT16 |
|---|---|---|---|
| $c_1$ | | 1.40E-04 | |
| $c_2$ | | -42.2 | |
| $e_0$ | 0.528 | 0.513 | 0.466 |
| $e_c$ | | 0.425 | |
| related to | FWPT2 | FWPT3 | FWPT6 |
| $R^2$ | | 0.976 | |

(a)

| | |
|---|---|
| $a_{FX\_e'}$ | 55.9 |
| $\varepsilon_a$ | -3.81 |
| $n_{FX\_e'}$ | 4.90 |
| $\varepsilon_n$ | 2.76 |
| $m_{FX\_e'}$ | 0.303 |
| $\varepsilon_m$ | 0.89 |
| $Cr$ | 197 |
| $R^2$ | 0.992 |

(b)

Table 5. Parameters (a) of the e-function (Equation 11) of PPCT13, PPCT22 and PPCT16 (Huang, et al., 1998) and (b) the proposed WRC model (Equation 21), all obtained using $R^2$ maximization

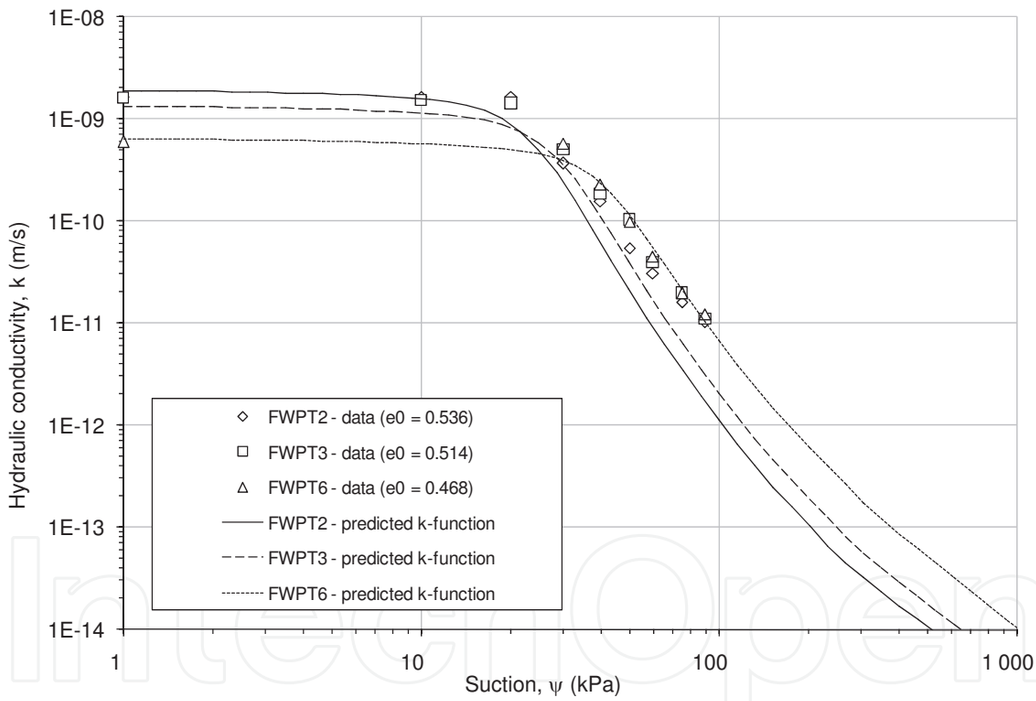


Fig. 16. Hydraulic conductivity function for Huang (1994)'s silty sand

The *k*-function of the silty sand was estimated using Equation 15 and Equation 16 based on the WRC determined using the proposed model. Parameters for equation Equation 15 are taken from Huang (1994). Since the derivative of the proposed model ($\theta'$ ; Equation 16) is rather complex to determine, the symbolic computation program *Maxima*[4] was used. The integrations were performed using quadratures in a *Scilab*[5] environment.

[4]http://maxima.sourceforge.net/

[5]Institut national de recherche en informatique et en automatique, France, Rocquencourt. http://www.scilab.org/

It can be observed that the *k*-functions are independent of each other, which is not the case of the WRC from which they derive. This is due to the intrinsic bias in Equation 16 associated with the supposition that the soil structure is incompressible (see section 2.3). However, the proposed WRC gives coherent *k*-function curves, the graphs being parallel on the log-log scale. The results in Fig. 16 show a rather good agreement between experimental data for FWPT6, but a much less good agreement for tests FWPT2 and FWPT3. Test FWPT6 underwent little shrinkage, which was not the case with FWPT2 and FWPT3. Equation 16 could be adapted for volume changes, using shrinkage factors, and a WRC model that considers volume changes, like the one proposed in this chapter. However, the development of a *k*-function model that considers shrinkage is beyond the scope of this report. The next section deals with application of the proposed model to the results of suction tests with DBP.

#### 4.1.1.2 Application of the proposed water retention curve model to deinking by-products

##### *4.1.1.2.1 The water retention curve of deinking by-products*

Fig. 17 presents the WRC data from suction tests with DBP performed in order to obtain the WRC (tests MCT1 to MCT4). The degrees of saturation data presented in Fig. 17 were obtained considering volume changes in the data reduction process. The proposed WRC model was employed to fit the four sets of experimental data. As shown in Fig. 12, the trend of parameter $a_{FX}$ against void ratio is closely related to whose of the air-entry value, both slopes being visually parallel. In Fig. 17, it can be observed that a good agreement results ($R^2$ = 0.875). It is shown in Table 6 that no variation was needed for parameters $n_{FX}$ , its slope being null.

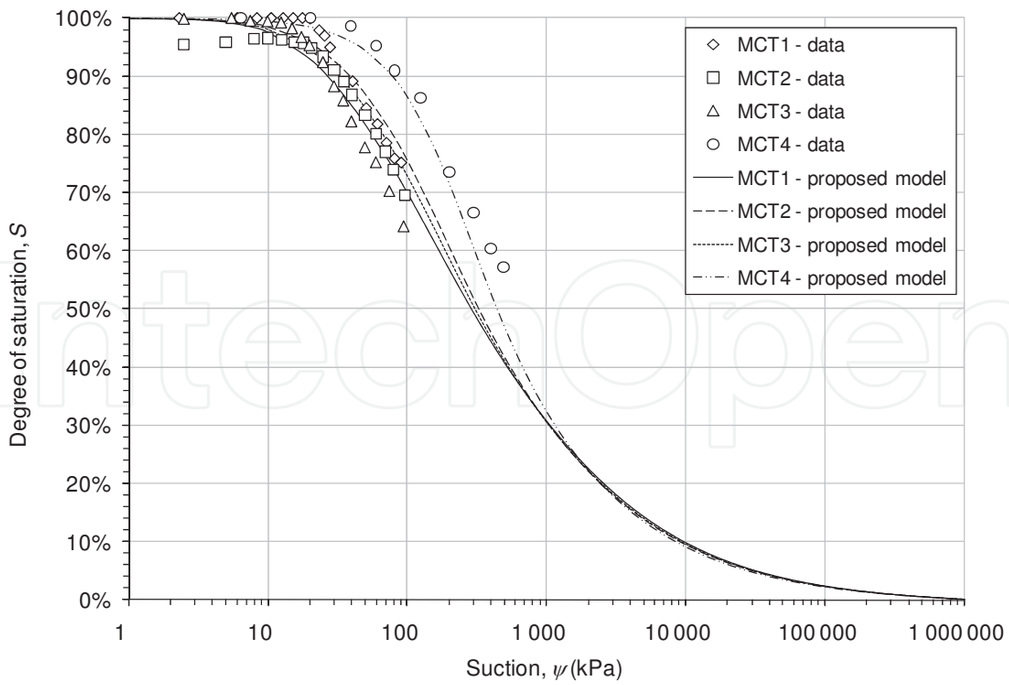


Fig. 17. Water retention curve for deinking by-products with consideration of volume change

| | |
|---|---|
| $a_{FX\_ec}$ | 1316 |
| $\varepsilon_a$ | -0.607 |
| $n_{FX\_ec}$ | 2.19 |
| $\varepsilon_n$ | 0.00 |
| $m_{FX\_ec}$ | 1.32 |
| $\varepsilon_m$ | -0.36 |
| $Cr$ | 1316 |
| $R^2$ | 0.875 |

Table 6. Parameters of the fitted WRCs

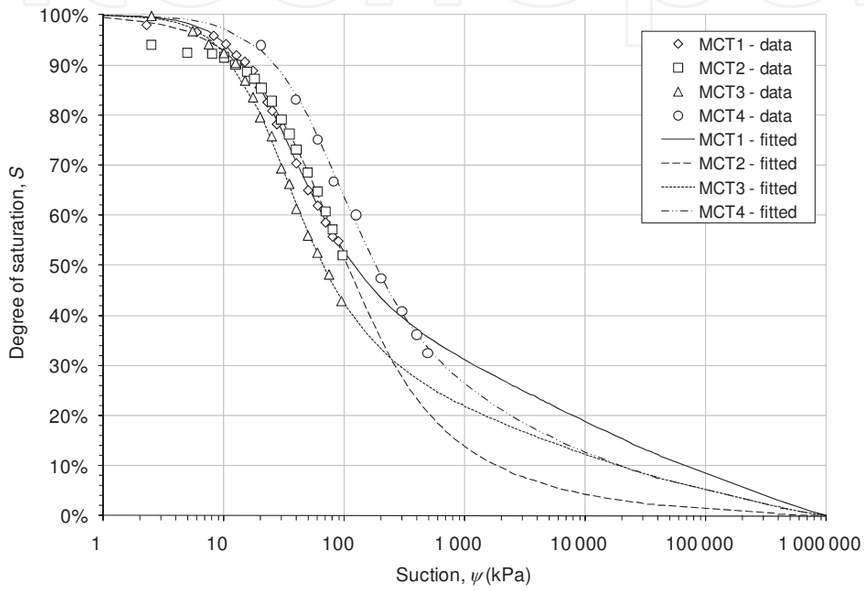


Fig. 18. Water retention curve for deinking by-products without consideration of volume change

| | MCT1 | MCT2 | MCT3 | MCT4 | Average | Standard deviation |
|---|---|---|---|---|---|---|
| $a_{FX}$ | 19.9 | 60.3 | 19.0 | 51.9 | 37.8 | 21.4 |
| $n_{FX}$ | 1.81 | 1.14 | 1.83 | 1.50 | 1.6 | 0.3 |
| $m_{FX}$ | 0.570 | 1.615 | 0.742 | 0.857 | 0.9 | 0.5 |
| $Cr$ | 3000 | 3000 | 3000 | 3000 | 3000.0 | 0.0 |
| $R^2$ | 0.998 | 0.999 | 0.999 | 0.997 | | |

Table 7. Parameters for the Fredlund & Xing (1994) water retention model for deinking by-products samples without consideration of volume change

If consideration is made that DBP do not undergo volume changes during application of suction, then the pore structure of the material would consequently remain unaltered. In this case, samples MCT1 to MCT4, which were consolidated to different initial void ratios, would behave as totally different materials. Fig. 18 presents suction test data for tests MCT1 to MCT4. The Fredlund & Xing (1994) model was used to fit experimental data, for which corrections due to volume changes in the data reduction process were not applied. Since

volume is considered to be constant, the sets of data were treated independently, i.e. the relevant parameters were optimized in an independent manner. The values of the several parameters, their average values and their standard deviations are shown in Table 6.

The experimental results in Fig. 19 clearly show that volumetric water contents are significantly underestimated if volume changes are not considered, particularly at high suction levels. For example, test MTC1, at approximately $\psi = 20\ kPa$, consideration of volume changes lead to a degree of saturation 14% greater than the value obtained if volume changes were not considered. At $\psi = 90\ kPa$, the difference increases to 20%.

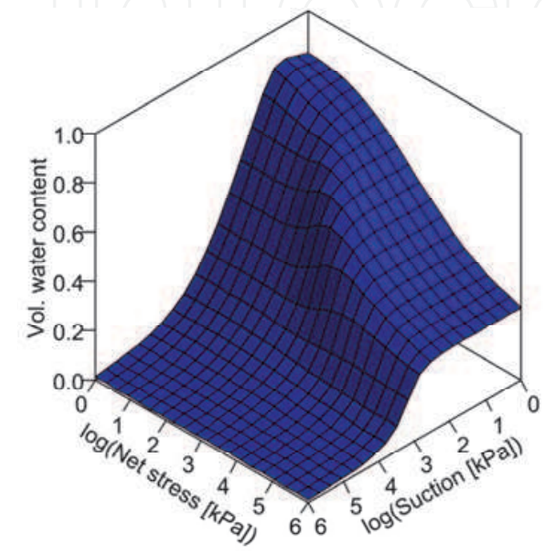


(a) MCT1

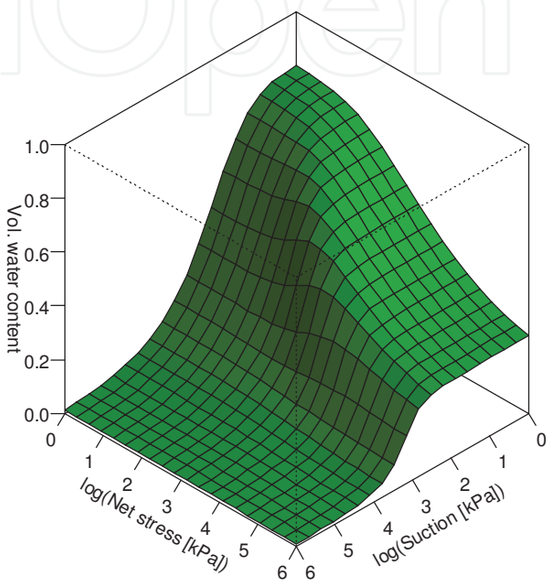


(b) MCT2

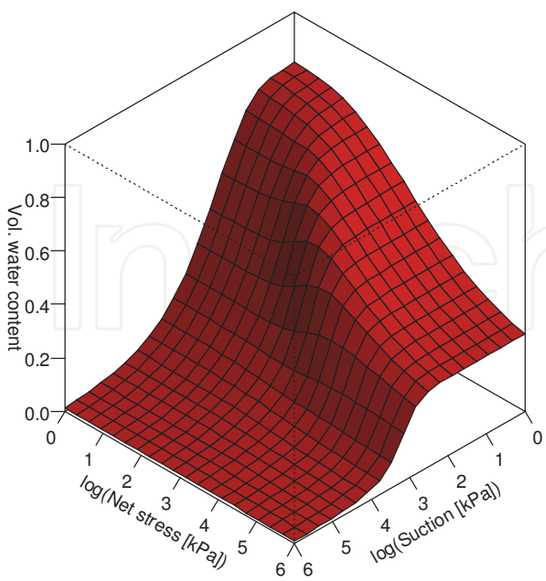


(c) MCT3

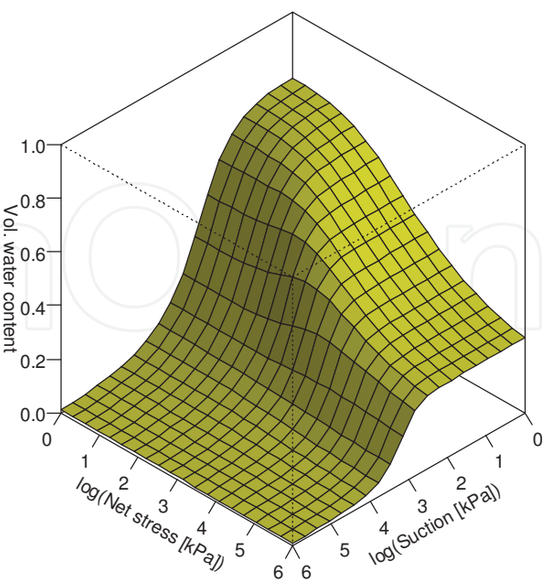


(d) MCT4

Fig. 19. Isometric representations of the water retention planes for tests MCT1 to 4

Since the void ratio is a function of both net stress and suction, and since the degree of saturation is a function of void ratio and suction, the degree of saturation can be plotted as a function of both net stress and suction in order to obtain water retention planes. Such three-dimensional representations may lead practitioners to better understandings of pore compression phenomena in unsaturated porous media.

#### *4.1.1.2.2 Hydraulic conductivity functions for deinking by-products*

Fig. 20 shows the hydraulic conductivity function (*k*-function) for tests MCT1 to MCT4. The curves were obtained based on their respective WRC that, in turn, were determined using the proposed model (Equation 21). Fig. 21 presents the *k*-functions for DBP based on the Fredlund & Xing (1994) WRC model (Equation 9 — no volume change), whose parameters are presented in Table 6. The value of $k_{sat}$ was determined based on the initial void ratio ($e_0$) of each test (Table 2).

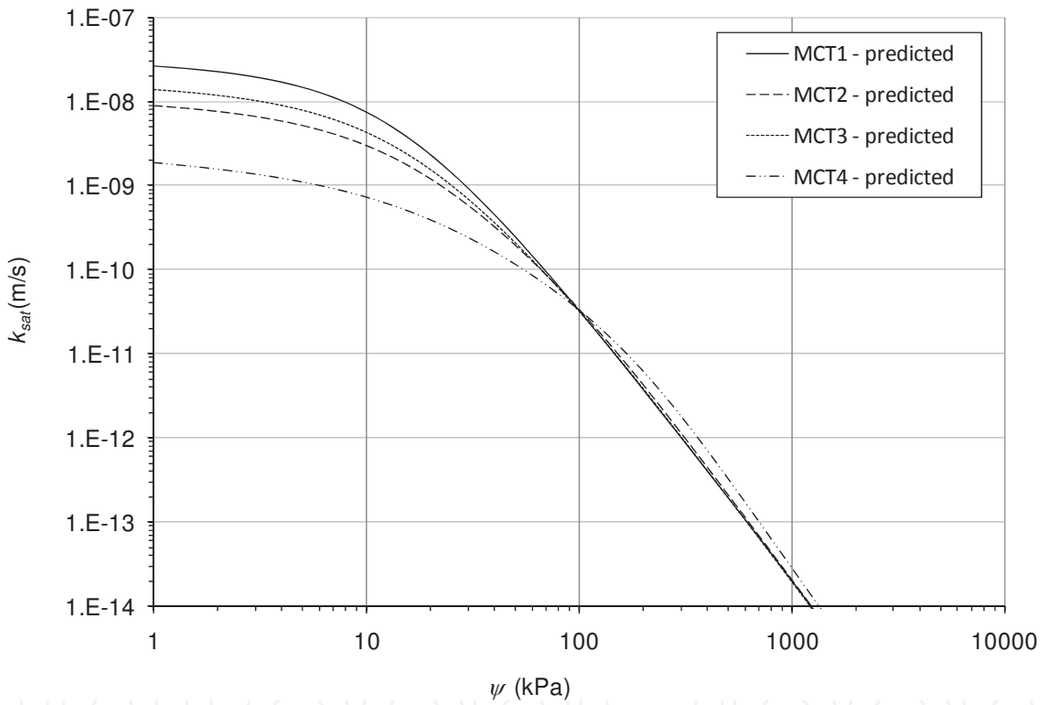


Fig. 20. Hydraulic conductivity functions for deinking by-products derived from models considering volume changes (proposed water retention curve model)

The different *k*-functions computed from the proposed model, plotted in Fig. 20, are closed to superimpose onto a single branch around a suction of 100 kPa, although the tendency of the void-ratio function (Fig. 15) and the degree of saturation (Fig. 18) shows a convergence around 1000 kPa. The bias in the computation of *k*-functions for HCMs (section 2.3) is still visible in Fig. 18, although barely apparent, perhaps because of the low standard deviation of porosity of DBP. This behavior is not observed in Fig. 21, where the four curves represent four independent samples Fig. 20 and Fig. 21 shows that the general trend of the *k*-function computed from the WRCs of respectively Fig. 18 and Fig. 19 is similar for both scenarios, although the *k*-function computed with the WRC that considers volume changes (Fig. 20) is more coherent with the theory (Fig. 5).

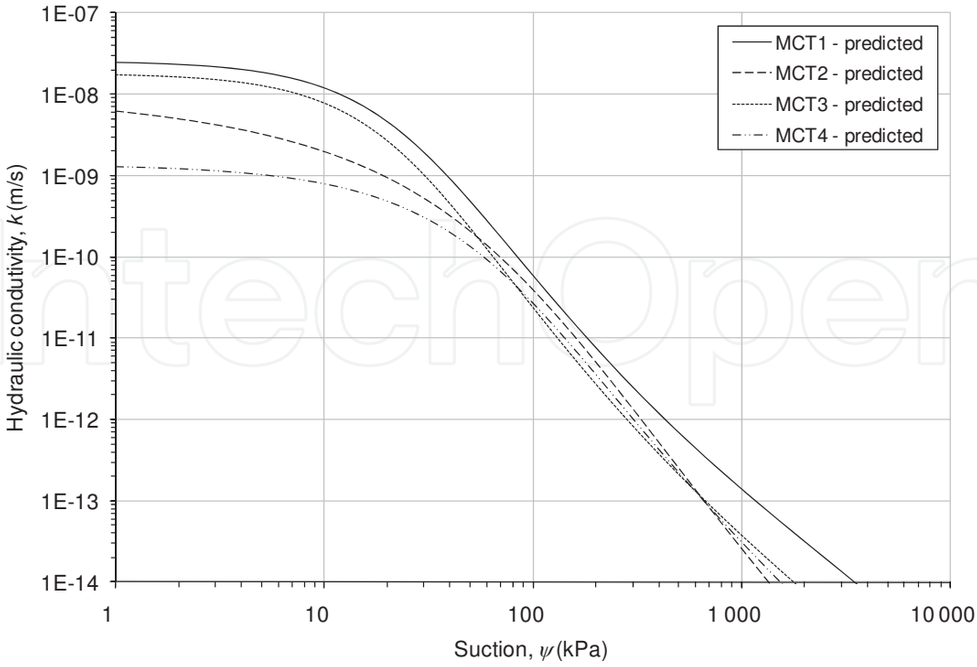


Fig. 21. Hydraulic conductivity functions for deinking by-products derived from models *not* considering volume changes (Fredlund & Xing (1994) water retention curve model)

#### 4.1.1.3 Model to predict the hydraulic conductivity function of a highly compressible material based on tests with saturated samples

The *k*-function predictive model presented below has the advantage over Fredlund & Xing (1994)'s model (Equation 16) to assume compressible structure and to be based on tests performed with saturated samples.

##### *4.1.1.3.1 The conceptual approach*

Fig. 22 can be utilized to explain the concept behind the proposed $k_{sat}$-$\psi_{aev}$ model. The *k*-function is described here by two curves. The first (denoted as curve 1) describes how the saturated hydraulic conductivity varies with suction for a sample of a highly compressible material consolidated to an initial void ratio $e_{0i}$. Using a void ratio function (*e*-function; proposed later), it is possible to predict the void ratio $e_i$ for any suction value $\psi$ and, using Equation 15, to predict the saturated hydraulic conductivity, $k_{sati}$, corresponding to $e_i$ and $\psi$. Although the curve in Fig. 15 extends beyond the AEV, obtainment *e* vs. $\psi$ curve beyond the AEV is not necessary for the purpose of determining curve 1 in Fig. 22. This is due to the fact that the value of $e_c$ does not affect significantly the value of $e_i$ for suctions lower than $\psi_{aevi}$, whether it is determined by a least square optimization technique or simply imposed based on a known residual value (as is the case in Fig.15). Using Equation 11 and the *e*-function, the AEV for test *i*, $\psi_{aevi}$, is then determined. The void ratio corresponding to $\psi_{aevi}$ is $e_{aevi}$.

The second curve (denoted as curve 3 in Fig. 22) can also be estimated based on saturated hydraulic conductivity tests and the WRC. For the same test *i* as above, consolidated to an initial void ratio $e_{0i}$, when suction exceeds $\psi_{aevi}$, the void ratio decreases to a value $e_{unsati}$ lower than $e_{aevi}$. Accordingly, the associated hydraulic conductivity decreases as expected to

a value $k_{unsati}$ lower than $k_{sati}$. This new hydraulic conductivity value, $k_{unsati}$, corresponds to the unsaturated hydraulic conductivity for sample *i* when its void ratio is $e_{unsati}$.

According to Equation 15, it is possible to obtain a saturated hydraulic conductivity corresponding to a void ratio $e_{unsati}$. In this case, another test *ii* (curve 2 in Fig. 22) must be performed using the same material, but the sample is consolidated to an initial void ratio $e_{0ii} < e_{0i}$. Suction is then applied to bring the sample to a void ratio $e_{aevii}$ equal to $e_{unsati}$ (Fig. 22).

Since, as shown schematically in Fig. 5, various WRCs superimpose into a single virgin desaturation branch Toll (1988) (this is equivalent to the consolidation behavior of clayey soils) and that the slope of the *k*-function can be calculated from the slope of the WRC, it may be inferred that *k*-functions also superimpose onto the same curve. Therefore, the curve obtained by joining the points ($\psi_{aev}$;$k_{sat}$) for tests *i*, *ii*, etc., *i.e.* curve 3 and 4 in Fig. 22, would describe the *k*-function of the compressible material for suctions greater than the AEV.

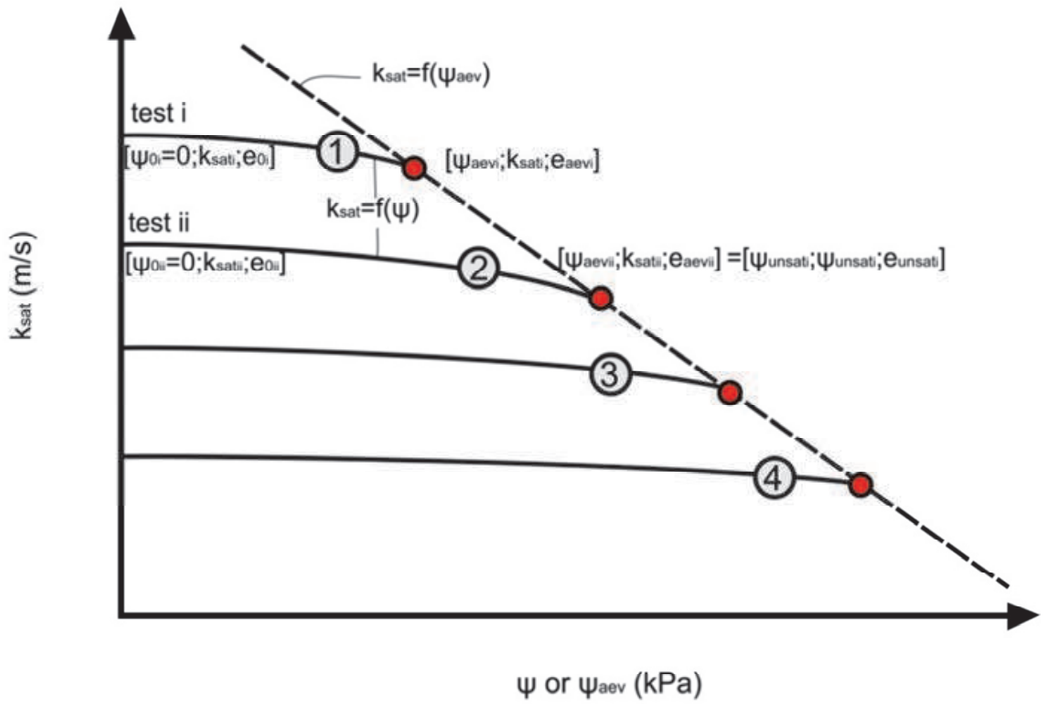


Fig. 22. Schematic representation of saturated hydraulic conductivity as a function of air-entry value

#### *4.1.1.3.2 The proposed procedure*

By substituting *e* in Equation 15 by $e_i$ obtained from Equation 20, the following model for curve 1 (or curve 2) is obtained as follows:

$$k_{sat_i} = k_{sat_i} 10^{b(e_c+(e_{oi}-e_c)(1+c_1 e_{oi}\sigma')^{c_2}-e'_{aev})} \quad \text{for} \quad \psi < \psi_{aev_i} \tag{22}$$

Curve 3 (Fig. 22) is obtained by replacing the parameters *e* and *e'* in Equation 15 by, respectively, $e_{aev}$ and $e'_{aev}$, by isolating $e_{aev}$ in Equation 11 and finally by substituting Equation 11 into Equation 15. Equation 23 is then used to establish a linear relationship on a *log*–*log* scale between $k_{sat}$ and $\psi_{aev}$:

$$k_{sat} = k_{sat_{e'}} \left(\frac{\psi_{aev}}{\psi'_{aev}}\right)^{\frac{b}{\epsilon_a}} \quad \text{for } \psi_{aev} > \psi_{aev_i} \tag{23}$$

#### *4.1.1.3.3 Validation and discussion*

In order to validate the proposed procedure, Equation 22 and Equation 23 were applied to experimental data published by Huang et al. (1998). The results, presented in Fig. 23, are compared to unsaturated hydraulic conductivity measurements, also reported by Huang et al. (1998).

Hydraulic conductivity, suction and void ratio values obtained from flexible-wall permeability tests allowed for the determination of the parameters in Equation 22.

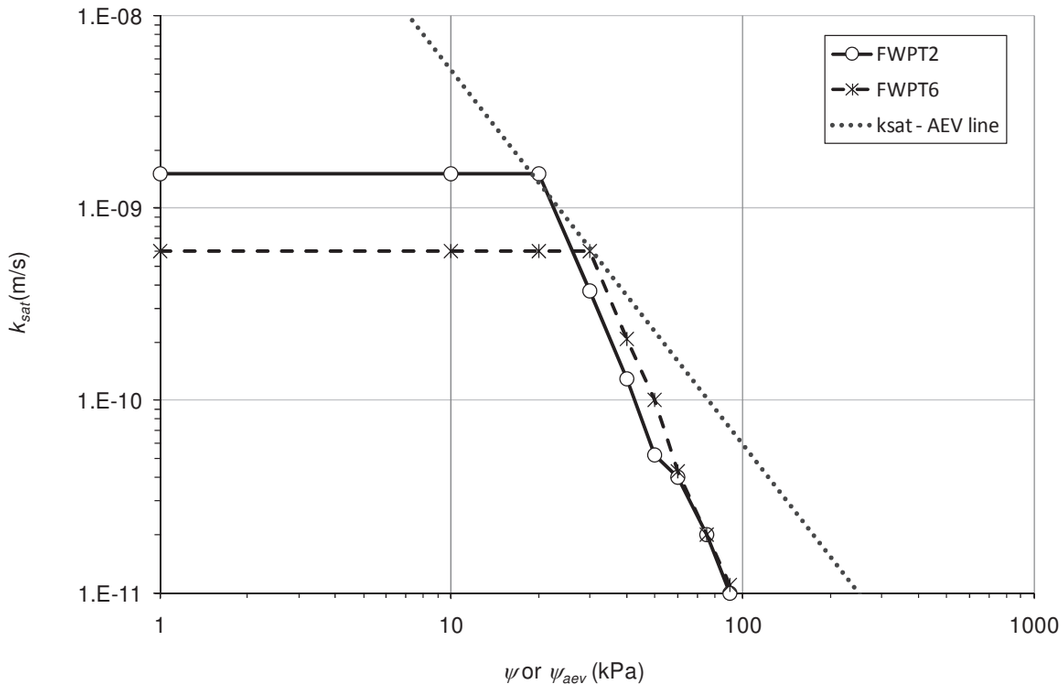


Fig. 23. Hydraulic conductivity as a function of suction using the $k_{sat} - \psi_{aev}$ model

Parameters $\psi'_{aev}$ and $\epsilon_a$ were obtained using results of pressure-plate cell tests, from which the curve $log(\psi_{aev})$ *vs.* $e_{aev}$ could in turn be determined.

Up to 30 *kPa* of suction, a good agreement also exists with results from flexible-wall hydraulic conductivity tests (squares in Fig. 23). It can be observed in figure Fig. 23 that the differences between the proposed procedure and the data best fit are relatively minor up to $\psi_{aevi}$. The model overestimated $k_{sat}$ by less than an order of magnitude at 90 *kPa*. This suggests that the determination of the *k*-function can be made based on known relationships between $k_{sat}$ and void ratio, and $\psi_{aev}$ and void ratio with reasonable confidence.

#### *4.1.1.3.4 Application of the $k_{sat}$-$\psi_{aev}$ model to deinking by-products*

Data from tests performed for DBP (Fig.8, Fig.15 and Fig. 13) were used to apply the $k_{sat}$-$\psi_{aev}$ model. Results are shown is Fig. 24 for tests MCT1 and MCT4. For test MCT1, at 10 *kPa*, the hydraulic conductivity obtained using the proposed WRC and Fredlund & Xing (1994)'s

model is twice as large as the one obtained using the $k_{sat}$-$\psi_{aev}$ model. For test MCT4, hydraulic conductivities predicted using both models are similar for suction values lower than 400 *kPa*; for higher suction values, hydraulic conductivities obtained using the $k_{sat}$-$\psi_{aev}$ model are higher than the ones obtained using the proposed WRC and Fredlund & Xing (1994)'s model, the *k*-function slope being steeper for the latter model than for the $k_{sat}$-$\psi_{aev}$ model.

The discrepancies between the two predictions may be caused by the lack of data available. It can be observed in Fig. 20 and Fig. 23 that the $k_{sat}$-$\psi_{aev}$ model overestimates the data and the prediction from the proposed WRC model.

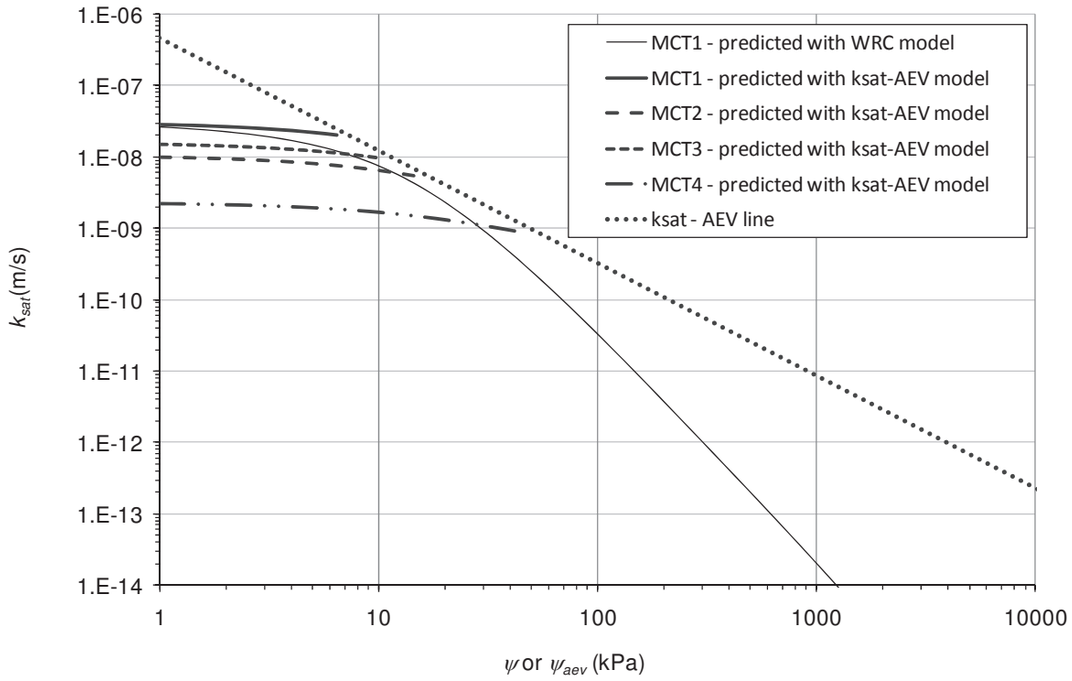


Fig. 24. Hydraulic conductivity functions for deinking by-products derived from the $k_{sat}$-$\psi_{aev}$ model

## 5. Conclusion

The hydraulic properties of DBP were determined using the experimental procedure described by Cabral et al. (2004) and water retention curve (WRC) and hydraulic conductivity function (*k*-function) models considering suction-induced shrinkage developed by the authors Parent et al. (2006; 2004).

### 5.1 The compression energy concept

Although energy units are used in soil compaction studies, the concept of compression energy is not used often in geotechnics. A stress is a concentration of energy describing the action of compression exerted on the pore network. The energy paradigm links the WRC, the porosity function and Bishop (1959)'s parameter χ. It was demonstrated in this chapter that the capillary induced compression energy may be important even for suction values

larger than the air-entry value (AEV). As a result, materials like DBP shrink over a large range of suction values beyond the AEV.

### 5.2 Model to determine the water retention curve of a highly compressible material

A model was proposed to describe the WRC of highly compressible materials (HCMs). The input parameters needed for the model were obtained directly from water retention tests. The experimental procedure used allowed to determine WRCs of materials undergoing significant volume changes during application of suction, i.e. HCM. Volume change in specimen was monitored during suction application, so that volumetric water contents can be continuously calculated.

The proposed WRC model was validated using published experimental data from tests performed with a compressible silty sand from Saskatchewan, Canada. Hydraulic conductivity functions (*k*-functions) based on the proposed WRC model fitted hydraulic conductivity values obtained from unsaturated permeability testing with this silty sand only for the data set that underwent no significant volume change, verifying the model bias of Fredlund et al. (1994)'s model (Equation 16) for HCM explained in section 2.3 As a result, there is a need for an accurate model able to predict the *k*-function of a HCM.

The proposed WRC model was applied to experimental data from representative tests on DBP. The proposed model fits experimental data with good accuracy ($R^2 = 0.902$). Volumetric water contents were significantly underestimated if volume change was eluded in the data reduction process.

Void ratio of DBP specimens tended to converge to the same value as suction increase. Consequently, their *k*-functions should also superimpose. Based on their respective WRC curve parameters, the *k*-functions for several tests were predicted using the Fredlund et al. (1994) model coupled with function that allowed variation in saturated hydraulic conductivity with void ratio. The *k*-functions obtained when the WRC model accounted for volume change converged to a single value at 10 000 *kPa*, even though the Huang et al. (1998) model was found to be inaccurate for HCM. On the other hand, if volume change was not accounted for, several independent *k*-functions were obtained.

We expect that the proposed WRC model could be applied to other compressible materials and that reliable *k*-functions could be derived using an appropriate *k*-function model. The appropriate parameters for the WRC must be obtained based on an experimental procedure such as the one presented in this paper. Further studies should also take into account the influence of hysteresis.

### 5.3 A model to predict the hydraulic conductivity function with saturated samples

A procedure to determine the *k*-function based on relationships between saturated hydraulic conductivity and void ratio, and between AEV and void ratio was developed and applied to DBP. A comparison between the *k*-function obtained by applying this procedure to experimental data reported in the literature (for a Saskatchewan silty sand) and actual unsaturated hydraulic conductivity data for the same silty sand shows a good agreement up to a suction value in the vicinity of 30 *kPa*. For higher suctions a reasonable agreement (less than one order of magnitude) is still obtained.

The use of the proposed procedure to determine the *k*-function requires suction and saturated hydraulic conductivity testing on samples consolidated to different initial void ratios.

However, these tests are more expeditious than direct determination of *k*-functions. Hence, the $k_{sat}$-$\psi_{aev}$ procedure may be a valuable and cost-effective solution in many situations.

## 6. References


Abdolahzadeh, A., Vachon, B., & Cabral, A. (2008). Hydraulic barrier and its impact on the performance of cover with double capillary barrier effect. *61e Conférence géotechnique canadienne.* Edmonton.

Abdolahzadeh, A., Vachon, B., & Cabral, A. (2010). submitted. Assessment of the design of an experimental cover with capillary barrier effect using four years of field data. *Geotechnical and Geological Engineering Journal* .

Arya, L., & Paris, J. (1981). A physicoempirical model to predict the soi1 moisture characteristic from particle-size distribution and bulk density data. *Soil Science Society of America Journal , 45*, pp. 1023-1030.

Aubertin, M., Mbonimpa, M., Bussiere, B., & Chapuis, R. (2003). A model to predict the water retention curve from basic geotechnical properties. *Fourth International Conference on Acid Rock Drainage*, *2*, pp. 731-746. Vancouver, Canada.

Audet, C., Lefebvre, G., Cabral, A., & Burnotte, F. (2002). State of development in the valorization of deinking by-products as an alternative to fine grained soils. *TAPPI.* Montréal, Canada.

Barbour, S. (1998). Nineteenth canadian geotechnical colloquium: The soil-water characteristic curve: a historical perspective. *Canadian Geotechnical Journal , 30* (5).

Baumgartl, T., & Kock, B. (2004). Modeling volume change and mechanical properties with hydraulic models. *Soil Science Society of America Journal , 68* (1), pp. 57-65.

Bédard, D. (2005). *Effet du fluage à long terme des sous-produits de désencrage dû à la perte de masse et son effet sur la compression et la conductivité hydraulique (Effect of creep of DBP due to mass loss and impact on the compressibility and hydraulic conductivity).* Master thesis, Université de Sherbrooke, Sherbrooke.

Bishop, A. (1959). The principle of effective stress. *Teknisk Ukeblad , 106*, pp. 859-863.

Bloemen, G. W. (1983). Calculation of the hydraulic conductivities and steady-state capillary rise in peat soils from bulk density and solid matter volume. *Zeitschrift für Pflanzenernährung und Bodenkunde , 146* (5), pp. 460-473.

Boivin, P., Garnierb, P., & Vauclin, M. (2006). Modeling the Soil Shrinkage and Water Retention Curves with the Same Equations. *Soil science society of America journal , 70*, pp. 1082-1093.

Brandyk, T., Szatylowicz, J., Oleszczuk, R., & Gnatowski, a. T. (2003). Water-related physical attributes of organic soils. In L. Parent, & P. Ilnìckì, *Organic Soils and Peat Material for Sustainable Agriculture* (pp. 33-66). CRC Press.

Brooks, R., & Corey, A. (1964). Hydraulic properties of porous media. *Hydrology paper, Colorado State University , 3*.

Burnotte, F., Lefebvre, G., Cabral, A., Audet, C., & Veilleux, A. (2000). Use of deinking residues for the final cover of a MSW landfill. *53rd Canadian Geotechnical Conference*, *1*, pp. 585-591. Montréal, Canada.

Cabral, A., Burnotte, F., Lefebvre, G., Amyot, G., & Lacasse, G. (1999). Design construction and monitoring of a waste rock cover using pulp and paper residues.

Cabral, A., El Ghabi, B., Parent, S.-É., & Marineau, L. (2007). Design and performance of an experimental double capillary barrier cover placed in a municipal solid waste landfill. *Proc. 11th Intern. Waste Mgmt and Landfill Symp., CD-Rom.* Cagliari.

Cabral, A., Lefebvre, G., Burnotte, F., Panarotto, C., & Pastore, E. (1999). Use of pulp and paper residues as an alternative cover material to landfill and to acid generating tailings. *Seminario de Meio Ambiente em Industrias de Processo*, (pp. 56-70). Sao Paulo, Brazil.

Cabral, A., Planchet, L., Marinho, F. A., & Lefebvre, G. (2004). Determination of the soi1 water characteristic curve of highly compressible materials: Case study of pulp and paper by-product. *Geotechnical Testing Journal* .

Childs, E., & Collis-George, G. (1950). The permeability of porous materials. *Royal Society of London , Series A*, pp. 392-405.

DelAvanzi, E. (2004). *Unsaturated flow under increased gravitational field.* Boulder: University of Colorado at Boulder.

D'Onza, F., Gallipoli, D., Wheeler, S., Casini, F., Vaunat, J., Khalili, N., et al. (2010). In press. Benchmarking of constitutive models for unsaturated soils. *Géotechnique* .

Ettala, M. (1993). Quality of deinking sludge. *Journal of Environmental Science and Health , A28* (4), pp. 923-932.

Fredlund, D. (1967). *Comparison of soil suction and one-dimensional consolidation characteristics of a highly plastic clay.* National Research Council Canada, Division of Building Research.

Fredlund, D., & Morgenstern, N. (1976). Constitutive relations for volume change in unsaturated soils. *Canadian Geotechnical Journal 13(3)* , 261-276.

Fredlund, D., & Rahardjo, H. (1993). *Soil mechanics for unsaturated soil.* New York, U.S.A.: Wiley.

Fredlund, D., & Xing, A. (1994). Equations for the soil-water characteristic curve. *Canadian Geotechnical Journal , 31* (4), pp. 521-532.

Fredlund, D., Xing, A., & Huang, S. (1994). Predicting the permeability function for unsaturated soils using the soil-water characteristic curve. *Canadian Geotechnical Journal , 31* (4), pp. 533-546.

Fredlund, M., Wilson, G., & Fredlund, D. (2002). Use of the grain-size distribution for estimation of the soil-water characteristic curve. *Canadian Geotechnical Journal , 39* (5), pp. 1103-1117.

Gallipoli, D., Gens, A., Sharma, R., & Vaunat, J. (2003). An elasto-plastic model for unsaturated soil incorporating the effect of suction and degree of saturation on mechanical behavior. *Géotechnique , 53* (1), pp. 123-135.

Holtz, R., & Kovacs, W. (1981). *Introduction to Geotechnical Engineering.*

Huang, S. (1994). *Evaluation and laboratory mesurment of the coeficient of permeability in deformable unsaturated soils.* Saskatoon, Department of civil engineering, University of Saskatchewan, Saskatchewan, Canada.

Huang, S., Barbour, S., & Fredlund, D. G. (1998). Development and verification of a coefficient of permeability function for a deformable unsaturated soil. *Canadian Geotechnical Journal , 35* (3), pp. 411-425.

Jardine, R., Standing, J., & Kovacevic, N. (2004). Lessons learned from full-scale observations and practical application of advanced testing and modelling. *Deformation Characteristics of Geomaterials. 2*, p. 45. IS-Lyon: Editions Di Benedetto.

Kamon, M., Inazumi, S., Rajasekaran, G., & Katsumi, T. (2002). Evaluation of waste sludge compatibility for landfill cover application. *Soils and Foundations* (42), pp. 13-27.

Kawai, K., Karube, D., & Kato, S. (2000). The model of water retention curve considering effects of void ratio. In H. Rahardjo, D. Toll, & E. Leong (Ed.), *Unsaturated Soils for Asia*, (pp. 329-334).

Kennedy, G., & Price, J. (2005). A conceptual model of volume-change controls on the hydrology of cutover peats. *Journal of Hydrology , 302*, pp. 13-27.

Khalili, N., & Khabbaz, M. (1998). A unique relationship for chi for the determination of shear strength of unsaturated soils. *Geotechnique , 48* (5), pp. 681-688.

Khalili, N., Geiser, F., & Blight, G. (2004). Effective stress in unsaturated soils: Review with new evidence. *International journal of Geomechanics , 4* (2), pp. 115-126.

Kraus, J., Benson, C., Maltby, C. V., & Wang, X. (1997). Laboratory and field hydraulic conductivity of three compacted paper mill sludges. *Journal of Geotechnical and Geoenvironmental , 123* (7), pp. 654-662.

Lapierre, C., Leroueil, S., & Locat, J. (1990). Mercury intrusion and permeability of louiseville clay. *Canadian Geotechnical Journal , 27*, pp. 761-773.

Latva-Somppi, J., Tran, H. N., Barham, D., & Douglas, M. A. (1994). Characterization of deinking sludge and its ashed residue. *Pulp and paper Canada , 2* (82), pp. 382-385.

Leong, E. C., & Rahardjo, H. (1997). Review of soil-water characteristic curve equations. *Journal of Geotechnical and Geoenvironmental Engineering , 123* (12), pp. 1106-1117.

Leong, E., & Rahardjo, H. (1997). Permeability functions for unsaturated soils. *Journal of Geotechnical and Geoenvironmental Engineering , 123* (12), pp. 1118-1126.

McCartney, J., & Zornberg, J. (2005). The centrifuge permeameter for unsaturated soils. In A. Tarantino, E. Romero, & Y. Cui (Ed.), *Advanced Experimental Unsaturated Soi1 Mechanics - Proceedings of an International Symposium.* Trento, Italy.

Moo-Young, H., & Zimmie, T. (1996). Effects of freezing and thawing on the hydraulic conductivity of paper mill sludges used as landfill covers. *Canadian Geotechnical Journal , 33*, pp. 783-792.

Mualem, Y. (1976). A new mode1 for predicting the hydraulic conductivity of unsaturated porous media. *Water Resources Research , 12*, pp. 513-522.

Nemati, M., Caron, J., & Gallichand, J. (2000). Using paper de-inking sludge to maintain soil structural form: Field measurements. *Soil Science Society of America Journal , 66* (2), pp. 367-373.

Nemati, M., Caron, J., Banton, O., & Tardif, P. (2002). Determining air entry value in peat substrates. *Soil Science Society of America Journal , 64* (1), pp. 275-285.

Ng, C., & Pang, Y. (2000). Influence of stress state on soil-water characteristics and slope stability. *Journal of Geotechnical and Geoenvironmental Engineering , 126* (2), pp. 157-166.

Nuth, M., & Laloui, L. (2008). Advances in modelling hysteretic water retention curve in deformable soils. *Computers and Geotechnics , 35* (6), pp. 835-844.

Nuth, M., & Laloui, L. (2008). Effective Stress Concept in Unsaturated Soils :Clarification and Validation of an Unified Framework. *International Journal of Numerical and Analytical Methods in Geomechanics , 32*, pp. 771-801.

Panarotto, C., Cabral,. A., Burnotte, F., Pastore, E., & Lefebvre, G. (1999). Utilisation des résidus de désencrage du papier comme recouvrement pour le contrôle du DMA: capacité de neutralisation de l'acidité résiduelle. *Congrès APGGQ*, (pp. 31-44). Rouyn-Noranda, Quebec, Canada.

Panarotto, C., Cabral, A. R., & Lefebvre, G. (2005). Environmental, geotechnical, and hydraulic behaviour of a cellulose-rich by-product used as alternative cover material. *Journal of environmental engineering and science , 4*, pp. 123-138.

Paquet, J., & Caron, J. (1993). In situ determination of the water desorption characteristics of peat substrates. *Canadian Journal of Soil Science , 73* (3), pp. 329-339.

Parent, S. (2006). *Hydraulic and geotechnical aspects of capillary barrier design using a highly compressible recylced material.* Sherbrooke: Ph.D. Thesis.

Parent, S., Cabral, A., Dell'Avanzi, E., & Zornberg, J. (2004). Determination of the Hydraulic Conductivity Function of a Highly Compressible Material Based on Tests with Saturated Samples. *Geotechnical Testing Journal , 27* (6), pp. 1-5.

Planchet, L. (2001). Utilisation des résidus de désencrage comme barrière capillaire et évapotranspirative (ÉT) pour les parcs à résidus miniers producteurs de DMA. Sherbrooke: Université de Sherbrooke.

Price, J., & Schlotzhauer, S. (1999). Importance of shrinkage and compression in determining water storage changes in peat : the case of a mined peatland. *Hydrological Processes , 13* (16), pp. 2591-2601.

Ratkowski, D. (1990). *Handbook of nonlinear regression model.* New York: M. Dekker.

Robart, G. (1998). *Étude de la perméabilité et de la compressibilité des résidus de désencrage (Studyof the permeability and compressibility of deinking residues).* Sherbrooke: Université de Sherbrooke.

Rode, P. C. (1990). Transient caluculation of moisture migration using a simplified description of hysteresis in the sorption isotherms. *Proceedings of the second symposium on building physics in the nordic countries.* Norwegian University of Science and Technology, Trondheim.

Roscoe, K., & Burland, J. (1968). *On the generalized stress-strain framework of "wet" clay* (Heymann and Leckie ed.). Cambridge: Cambridge University Press.

Salager, S., El Youssoufi, M., & Saix, C. (2010). Definition and experimental determination of a soil-water retention surface. *Canadian Geotechnical Journal , 47* (5), pp. 609-621.

Schlotzhauer, S., & Price, J. (1999). Soil water flow dynamics in a managed cutover peat field, Quebec: Field and laboratory investigations. *Water Resources Research , 35* (12), pp. 3675-3683.

Simms, P., & Yanful, E. (2002). Predicting soil-water characteristic curves of compacted plastic soils from measured pore-size distributions. *Geotechnique , 54* (4), pp. 269-278.

Smith, K., & Mullins, C. (2001). *Soil and environmental analysis : physical methods, 2nd edition.* M. Dekker.

Terzaghi, K. (1936). A Fundamental Fallacy in Earth Pressure Computations. *Journal of Boston Society of Civil Engineers , 23*, pp. 71-88.

Toll, D. (1995). A conceptual model for the drying and wetting of soils. In *Unsaturated Soils* (Vol. 2).

Toll, D. (1988). *The behaviour of unsaturated compacted naturally occurring gravel.* University of London: Ph.D. Thesis.

Tripathy, S., Rao, K., & Fredlund, D. (2002). Water content - void ratio swell-shrink paths of compacted expansive soils. *Canadian Geotechnical Journal , 39* (4), pp. 938-959.

van Genuchten, M. T. (1980). A closed-form equation for pre- dicting the hydraulic conductivity of unsaturated soils. *Soil Science Society of America Journal , 44*, pp. 892-898.

van Genuchten, M., Leij, F., & Yates, S. (1991). *The RETC Code for Quantifying the Hydraulic Functions of Unsaturated Soils, Version 1.0.* Riverside, California: EPA Report 600/2-91/065, U.S. Salinity Laboratory, USDA, ARS.

Vanapalli, S., Fredlund, D., & Pufahl, D. E. (1999). The influence of soil structure and stress history on the soil-water characteristics of a compacted till. *Geotechnique , 49* (2), pp. 143-159.

Vlyssides, A. G., & Economides, D. G. (1997). Characterization of wastes from a newspaper wash deinking process. *Frenesius Environ. Bull. , 6*, pp. 734-739.

Weiss, R., Alm, J., Laiho, R., & Laine, J. (1998). Modeling moisture retention in peat soils. *Soil Science Society of America Journal , 62* (2), pp. 305-313.

Zhou, J., & Yu, J.-l. (2005). Influences affecting the soil-water characteristic curve. *Journal of Zhejiang University SCIENCE, 6A* (8), pp. 797-804.

Zhuang, J., Jin, Y., & Miyazaki, T. (2001). Estimating water retention characteristic from soil particle-size distribution using a non-similar media concept. *Soil Science, 166* (5), pp. 308-321.

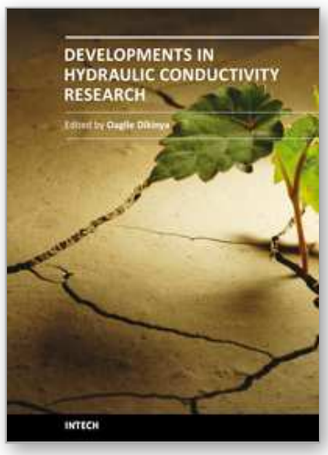


**Developments in Hydraulic Conductivity Research**

Edited by Dr. Oagile Dikinya

ISBN 978-953-307-470-2
Hard cover, 270 pages
**Publisher** InTech
**Published online** 28, February, 2011
**Published in print edition** February, 2011

This book provides the state of the art of the investigation and the in-depth analysis of hydraulic conductivity from the theoretical to semi-empirical models perspective as well as policy development associated with management of land resources emanating from drainage-problem soils. A group of international experts contributed to the development of this book. It is envisaged that this thought provoking book will excite and appeal to academics, engineers, researchers and University students who seek to explore the breadth and in-depth knowledge about hydraulic conductivity. Investigation into hydraulic conductivity is important to the understanding of the movement of solutes and water in the terrestrial environment. Transport of these fluids has various implications on the ecology and quality of environment and subsequently sustenance of livelihoods of the increasing world population. In particular, water flow in the vadose zone is of fundamental importance to geoscientists, soil scientists, hydrogeologists and hydrologists and allied professionals.

**How to reference**

In order to correctly reference this scholarly work, feel free to copy and paste the following:

Serge-Étienne Parent, Amir M. Abdolahzadeh, Mathieu Nuth and Alexandre R. Cabral (2011). Hydraulic Conductivity and Water Retention Curve of Highly Compressible Materials- From a Mechanistic Approach through Phenomenological Models, Developments in Hydraulic Conductivity Research, Dr. Oagile Dikinya (Ed.), ISBN: 978-953-307-470-2, InTech, Available from: http://www.intechopen.com/books/developments-in-hydraulic-conductivity-research/hydraulic-conductivity-and-water-retention-curve-of-highly-compressible-materials-from-a-mechanistic

INTECH
open science | open minds

**InTech Europe**
University Campus STeP Ri
Slavka Krautzeka 83/A
51000 Rijeka, Croatia
Phone: +385 (51) 770 447
Fax: +385 (51) 686 166
www.intechopen.com

**InTech China**
Unit 405, Office Block, Hotel Equatorial Shanghai
No.65, Yan An Road (West), Shanghai, 200040, China
中国上海市延安西路65号上海国际贵都大饭店办公楼405单元
Phone: +86-21-62489820
Fax: +86-21-62489821

IntechOpen